Investigation of Improved Hall Thruster Configurations for Low Power Operation

Research Thesis

Submitted in Partial Fulfillment of the Requirement for the Degree of Master of Science

By

Shlomy Shitrit

Submitted to the Senate of the Technion – Israel Institute of Technology

Nisan, 5765 HAIFA May 2005

Acknowledgments

First and foremost I would like to thank my technician, Mr. Gabi Appelbaum, both for his great experience and limitless patience. Thank you for hours of fruitful discussions.

I would like to express my sincere gratitude to my advisor, Dr. Joseph Ashkenazy, who has provided me an outstanding guidance. He was an invaluable resource throughout my research at Soreq.

I want to thank my advisor in the technion, professor Benny Natan, who supported me through all the way.

I also would like to thank everyone in Propulsion field – Avner Adany, Zilberman, Eyal, Pavel and Ortal, you have all have played a positive and integral role in my experience here. Thank you for making Soreq NRC, a fun place to work.

Special thanks to Prof. Amnon Fruchtmann, for a fruitful collaboration and helpful discussions.

Finally, I would like to thank Avi Warshavsky and Leonid Rabinovich from Rafael/Manor for a fruitful collaboration.

Table of Contents

List of Figures and Tables

Abstract

The Hall thruster generates its thrust by accelerating a plasma jet by the combined operation of perpendicular electric and magnetic fields in a coaxial channel. It can achieve a very high specific impulse, 1000-3000 sec, and thus its use in space missions will lead to large savings in the required propellant mass. The capability of changing their performances by varying parameters such as discharge voltage or mass flow rate makes Hall thrusters ideal for missions where different types of maneuvers require different levels of thrust and specific impulse. This work deals with the performance of low power (200-300W) Hall thrusters. The problem of the degradation of Hall thruster performance, when a given thruster configuration is operated at reduced power levels, is analyzed. Results of experiments performed with a Hall thruster in the 200-600 Watts power range demonstrate this type of degradation. It is explained as being a result of the drop in the efficiency of the ionization process at reduced propellant flow rates. The standard approach to overcome this problem by scaling down the thruster is analyzed and proper scaling rules are outlined. It is demonstrated however that the proper implementation of the required scaling is limited by magnetic material and circuit properties. It is also shown that the main drawback of down sized Hall thrusters in the power range below 300 Watts is the sharp drop in their operating lifetime compared to larger size thrusters. As a consequence, a different approach, to try to improve the propellant utilization by geometric or magnetic modifications but without scaling down the thruster, is preferred for Hall thrusters in the 200-300 Watts power range. The straightforward implementation of this approach, by extending the channel length was investigated experimentally. As part of this investigation, an improved laboratory Hall thruster has been designed and constructed. In order to improve the thrust measurement accuracy and, as well, to reduce uncertainties related to the conditions inside the vacuum chamber during cryopumps and thruster operation, a new calibration system, which allows to calibrate the thrust stand at vacuum conditions and during thruster operation, was designed and built. By using the new calibration system the relative error in the thrust measurement was reduced from 3.1% to ~1.9% (thrust of 12mN). The channel length investigation comprised of an extensive parametric study of thruster performance at five length configurations. Results of the experimental testing indicate that in the 200-350W input power range, higher thrust, specific impulse and efficiency are achieved when the length is extended from 33mm to 40mm, e.g. in an input power of 270W, the thrust is improved from 13mN to

15mN, corresponding to improvements in the specific impulse and thruster efficiency from 1325sec to 1450sec and from 30.5% to 37.8%, respectively. However, when the channel was further extended, only minor performance differences were observed, in the input power range of 250-350W. The effect of the magnetic field distribution on the thruster performance at reduced mass flow rates was also examined. This part of the work included a preliminary investigation of a novel idea of a new type of Hall thruster, which uses a reversed magnetic field near the anode, in order to improve the ionization efficiency and at the same time to increase the magnetic field gradient near the channel exit and thus, allow a better focusing of the plume which hopefully may lead to higher thruster efficiencies. In order to implement a reversed magnetic field configuration, a modified magnetic circuit was built and tested. Preliminary results demonstrated that indeed this configuration operated as a thruster although at somewhat lower thrust levels (0.5-2mN). On the other hand there were some indications for a better focusing of the jet with this configuration.

Nomenclature

m_e	Electron mass [kg]
m_i	Ion mass [kg]
$\dot{m}_a$	Anode mass flow rate [kg/s]
$\dot{m}_c$	Cathode mass flow rate [kg/s]
n_e	Electron density [$1/m^3$]
n_i	Ion density [$1/m^3$]
P_e	Discharge power [W]
q_i	Ion charge [C]
R_{Le}	Electron Larmor radius [m]
R_{Li}	Ion Larmor radius [m]
T	Thrust [mN]
e	Electron charge [C]
g	Gravitational acceleration [m/s^2]
I_d	Discharge current [A]
I_i , I_e	Ion and Electron current [A]
Isp	Specific impulse [sec]
k	Boltzmann constant [J/K]
B	Magnetic field [Gauss]
B_r , B_z	radial and axial magnetic field [Gauss]
T_e	Electron temperature [eV, K]
v_e	Electron velocity [m/s]
η_T	Thruster efficiency
ϕ	Discharge potential [V]
η_i	Ratio of the ion current to the discharge current
η_v	Voltage utilization at the thruster exit
η_p	Propellant utilization
v_i	Ion velocity [m/s]
l_a	Acceleration length where the main discharge voltage is established
E	Electric field [V/m]
E_r , E_z	radial and axial electric field [V/m]
v_ϑ	Azimuthally electron velocity [rad/s]
v_z	Axial electron velocity [m/s]
w_e	Electron cyclotron frequency [rad/s]
τ	Time between electron collisions [sec]
λ_i	Characteristic ionization length [m]
v_{jet}	Jet velocity [m/s]

$\mathfrak{R}_i, \mathfrak{R}_g$ Iron core and gap reluctance [amper-turn/weber]

Chapter 1

Introduction

1.1 Electrical Rocket Propulsion

An electric thruster is a rocket engine which utilizes electric energy to generate the jet. Unlike conventional chemical rocket engines, the jet velocity of electric thrusters does not depend on the sound speed of combustion gases, which is limited by a typical chemical binding energy. Thus, electric thrusters can achieve a much higher specific impulse (Isp) than chemical thrusters, leading to large savings in the required propellant mass for a given mission. The high specific impulse of electrical thrusters is not without penalties. Since spacecraft is a power limited system, and since the specific impulse of the thruster is high, electric propulsion is limited to a low thrust level [1]. Nevertheless, for some on orbit missions, low thrust levels is an advantage. Low thrust levels may be used to provide more precise positioning and attitude control than higher thrust chemical devices [2, 3].

1.2 Missions of Electric Thrusters

Characterized by a large Isp and a small thrust, electric thrusters are most suitable for space applications, such as: station keeping, orbit transfer and interplanetary missions.

Station Keeping

Communication satellites are usually launched to geosynchronous earth orbit. This is a circular orbit around the equator, about 36000km above the earth, in which the angular velocities of the earth and the satellite are equals; therefore the satellite stays always above the same point on earth. The geosynchronous orbit is very sensitive to initial errors in launch and other perturbation that can occur in space. Inaccuracy in the velocity can cause the satellite to drift away from its calculated orbit. In order to overcome these problems and reduce the errors one can use small thrust engines. The present technology is based on hydrazine propellant. The Δv that requires to stabilize the orbit is 50m/sec per year [4], therefore satellite whose approximated lifetime is ten years needs a velocity

increment of 500m/sec. Satellite that weight 800kg (include the propellant mass) will consume 200kg of hydrazine (Isp≈170sec) in order to complete its mission. On the other hand an electric thruster with an Isp of ~2000sec will consume only 20kg of propellant. These savings can be realized by extending the lifetime of the satellite for a given propellant mass or increase the payload instead of the saved propellant [5].

Orbit Transfer

This mission is mainly characterized by transfer from low earth orbit (LEO), where a chemical rocket was needed in order to perform the launch from earth, to GEO or higher. An example of the expected propellant saving is presented in [4]: A satellite that weight 2300Kg will consume 13500Kg of chemical propellant in order to implement the LEO-GEO transfer. On the other hand, an electric thruster will consume only 900Kg of propellant to fulfill the mission. Due to the significant savings in the mass propellant, smaller chemical launcher is needed. If the size of the launcher is limited and as a result the payload on the rocket is limited too, electric thrusters may be the only option to launch the payload to high orbit.

Interplanetary Missions

The advantages of the electric propulsion will be realized in deep space missions, where high Δv is required. As an example let us investigate a journey from an orbit around the earth to mars and back to earth. A Δv of 14Km/sec is needed for a spacecraft in LEO [6]. If the spacecraft mass at the end of the mission is 10 ton, a chemical rocket with an Isp of ~400sec will consume 321.15 tons of propellant. On the other hand, an electric thruster with an Isp of ~1000sec will consume only 4.19 tons of propellant [6].

1.3 Types of Electric Thrusters

The research of electrical propulsion had been started in the United-States and Russia in the late 50's, at the beginning of the race to space. More efforts to develop such engines were taken in Japan and Europe (Germany, Italy, England, and France). Since then many concepts of electric thrusters have been proposed and followed by research and development efforts in many laboratories around the world. Basically, electric thrusters can be divided into three categories [7]:

Electrostatic: In this case the propellant consists of charged particles accelerated by electrostatic forces. The particles (atoms) can be ionized by electron bombardment or by RF. Historically in the West (U.S.A, Europe, Japan), the largest effort was devoted to the development of the electrostatic ion thruster [7]. The ion thruster can achieve a very high Isp (2000-4000sec) and a high efficiency (50%-80%) [8]. On the other hand, its thrust density is low due to the limited ion current density which results from space charge effects and from the damage to the accelerating electrodes caused by colliding ions. Ion propulsion has demonstrated more than 10000 hours of operation in the Deep Space 1 mission, in 2001 [9]. A peak thrust of 92mN was achieved corresponding to a specific impulse of 3200sec with about 2kW delivered to the power processing unit. The energy source was a solar photovoltaic array [10].

Electrothermal: Efforts were devoted to the development of the resistojet and arcjet electrothermal thrusters. In the first concept the propellant is heated by an electric resistor. The specific impulse is limited by the maximum temperature that the electrical body can resist. The first experiment with resistojet engine was done in 1965 and until 1986 this technology served on 25 satellites. The state of the art uses hydrazine and reaches Isp of 295sec and thrust force of 180-490mN. [11, 12]. The arcjet generates thrust by striking an electrical arc between two electrodes. The rapid heating expands the gas to generate high thrust. A 750W ammonia arcjet was used on the AMSAR P3-D radio satellite in 1996. The thruster accomplished a lifetime of 1010 hours with a thrust of 115 mN and a specific impulse of 480s [13].

Electromagnetic: In this application of electrical energy, a stream of plasma is accelerated by magnetic pressure forces. The use of magnetic fields enables to accelerate a quasi-neutral plasma and thus to avoid space charge problems. As a result, a thrust density much higher than the ion thruster is possible. An example of electromagnetic propulsion is the MPD thruster which consists of a central cathode surrounded by concentric anode. A high current is generated between the anode and cathode which ionizes and accelerates a gas propellant. There are two type of MPD thrusters: The first is a self field thrusters in which azimuthal magnetic field produced by the current through the cathode interacts with the radial discharge current through the plasma to produce an axial Lorentz force. In the applied field version of the thruster, a solenoid magnet

surrounding the anode provides additional radial and axial magnetic fields that can help stabilize and accelerate the plasma discharge.

1.4 The Hall Thruster

The Hall thruster can be regarded either as electrostatic or electromagnetic type of thruster. It is an engine in which an applied radial magnetic field is used together with an axial electric field to accelerate a quasi-neutral plasma jet in a coaxial channel. In this regard, the Hall thruster represents a combination of properties which makes it attractive relative to other types of electric propulsion: high specific impulse, as compared to electrothermal thrusters, and compactness, as compared to the ion engine. The state-of-the-art thrusters can have an Isp of 1000-3000sec and an efficiency of more than 50% [1]. In the former Soviet Union thrusters onboard satellites operated at sub-kilowatt power level and also at 1.35KW, while additional models at up to 25KW have reached various stages of development [14]. The Hall thruster is capable of changing its thrust and specific impulse by varying parameters such as discharge voltage and mass flow rate. This capability makes them ideal for missions where different types of maneuvers require different thrust levels and specific impulse.

1.4.1 Principle of Operation

The Hall thruster is a coaxial device in which a magnetic field that is produced by an electromagnet is directed between the inner and outer magnetic poles. In Figure 1.1 a schematic drawing of the Hall thruster principle of operation is presented. This configuration has an essentially radial magnetic field with a peak of more than hundred Gauss, at the channel median near the exit plane. This field strength is such that the heavy ions experience negligible influence due to the magnetic field while the trajectory of the much lighter electrons is significantly affected. In addition to the applied magnetic field an axial electric field is provided by applying a voltage between the annular anode and the cathode. As the electrons proceed from the cathode to the anode, under the influence of the electric field, the magnetic field configuration results in an $\vec{E} \times \vec{B}$ drift in the azimuthal direction impeding their progress to the anode. The electrons are trapped in a closed drift azimuthal orbit with only collisions with ions, neutral particles and channel walls permitting a slow diffusion toward the anode. Propellant atoms (typically Xenon)

are injected into the discharge volume through multiple holes in the annular anode. Through collisions with the diffusing electrons these atoms are ionized. The ionized propellant is then accelerated by the large axial electric field, producing the thrust.

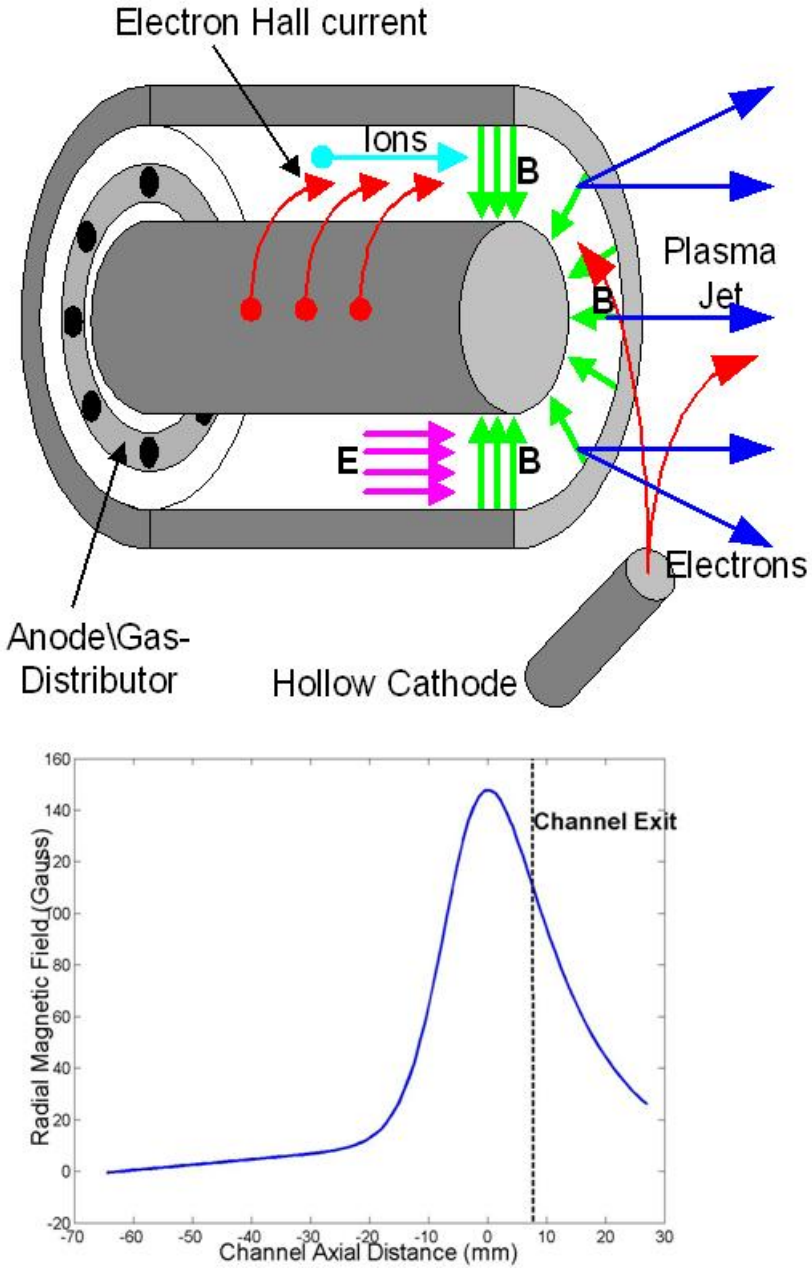

Figure 1.1: Schematic drawing of a conceptual Hall thruster. The azimuthal current of trapped electrons referred to as the Hall current. Also presented in the graph below the drawing is a typical radial magnetic field profile at the channel median.

In order for the magnetic field to have a strong effect on the electron path while having an insignificant effect on the ion motion, the length of the acceleration region, l_a , where most of the voltage drop occurs, has to be much larger than the electron Larmor radius,

R_{Le}, while at the same time has to be much smaller than the ion Larmor radius, R_{Le}. This condition is given as,

$$R_{Le} << l_a << R_{Li}, \tag{1.1}$$

where $R_{Le} = m_e \mathrm{v}_e / eB$ is the electron Larmor radius of gyration in a magnetic field B. e is the electron charge, m_e and v_e are the electron mass and average velocity, respectively. For a Xenon ion which is heavier than the electron (by about 250000) this condition is easily achieved. To see how the magnetic field can impede the electron motion, let us examine the equation of motion for a single electron in the presence of electric and magnetic fields:

$$m_e \frac{d\vec{\mathrm{v}}_e}{dt} = e(\vec{E} + \vec{\mathrm{v}}_e \times \vec{B}). \tag{1.2}$$

For an axial electric field, $\vec{E} = \hat{z}E$ and a radial magnetic field, $\vec{B} = \hat{r}B$, and taking $\mathrm{v}_e(t=0)=0$, we get:

$$\mathrm{v}_{e\theta} = \frac{E}{B}(1 - \cos(\omega_e t)), \tag{1.3}$$

$$\mathrm{v}_{ez} = -\frac{E}{B}\sin(\omega_e t), \tag{1.4}$$

$$\mathrm{v}_{er} = 0, \tag{1.5}$$

where $\omega_e = eB / m_e$ is the electron cyclotron frequency, r and z are the radial and axial coordinates respectively. The electron has an azimuthal velocity while its axial motion is limited to a Larmor radius.

In order to examine the ion acceleration process it is helpful to look at the plasma as composed of an electron fluid and an ion fluid. At steady state, the electron fluid equation of motion is given by [15]:

$$m_e n_e \{(\vec{\mathrm{v}}_e \cdot \nabla)\vec{\mathrm{v}}_e\} = -en_e(\vec{E} + \vec{\mathrm{v}}_e \times \vec{B}) - \nabla p_e - \frac{m_e n_e(\mathrm{v}_e - \mathrm{v}_i)}{\tau}. \tag{1.6}$$

$p_e = n_e k T_e$, is the electron pressure and τ is the electron mean time between ion-electron collisions through which the two fluids exchange momentum. The momentum loss per collision is proportional to the relative velocity, v_e-v_i, therefore we can write the contribution of the collision as $\mathrm{m}_e n_e(\mathrm{v}_e - \mathrm{v}_i)$. These collisions allow the electrons to diffuse towards the anode through the radial magnetic field lines. This particular motion

causes an axial electron current which bombards and ionizes the Xenon neutrals. The ratio of the inertial term on the left side of this equation to the Lorentz force term can be estimated as $\frac{1}{2} m_e v_e / e l_a B = \frac{1}{2} R_{Le} / l_a$, and thus the inertial term can be neglected. The Ohmic term, the last one on the right side, represents the force due to collisions of the electrons with ions. As the velocity of the lighter electrons is much larger than the ion velocity, the ratio of the Ohmic term to the Lorentz term can be approximated as $m_e / eB\tau = 1/\omega_e \tau$. $\omega_e \tau$ is the Hall parameter, representing the number of electron gyrations between collisions. In a typical Hall thruster the Hall parameter is much larger than unity, and so the Ohmic term can be neglected too. Finally we get:

$$E \approx -\mathrm{v}_e \times B - \frac{\nabla p_e}{e n_e}. \tag{1.7}$$

Assuming also that the plasma is cold, we obtain:

$$E \approx -\mathrm{v}_e \times B \Rightarrow E \cdot B \approx 0. \tag{1.8}$$

That is, the electric field and the magnetic field are perpendicular. This means that by impeding the electron flow the magnetic field distribution determine the distribution of the electric field that accelerates the ions. Since the effect of the Lorentz force on the ions is small, and the ion temperature is small, the ion equation of motion is written as:

$$m_i \frac{d\mathrm{v}_i}{dt} \approx eE(r,z), \tag{1.9}$$

where *E(r,z)* is the electric field distribution in *r,* θ and *z* directions. The electric and the magnetic fields are axisymmetric, reflecting the channel and the magnetic circuit geometry. It follows from Equation (1.9) that the thrust of the Hall thruster is due to the electrostatic acceleration of the ion through the channel exit.

From the two equations of motion one can see that the radial magnetic field, B_r, is responsible to the existence of an axial electric field which accelerates the ions, while an axial magnetic field component gives rise to a radial electric field and to transversal acceleration. In the case that the plasma is no longer cold and the electron temperature is no longer negligible, their radial pressure gradient causes an additional radial electric field which diverts the jet of the ions (see Eq. (1.7)).

1.4.2 Hall Thruster Performance

The thruster performance is determined by the thrust, *T*, the specific impulse, *Isp*, and the efficiency, η_T. The specific impulse is a type of fuel efficiency that evaluates the ability of the thruster to convert propellant into useful thrust, or in other words it describes the momentum gain per propellant mass element:

$$Isp = \frac{T}{\dot{m}g}, \tag{1.10}$$

where $\dot{m}$ is the propellant mass flow rate and g is the acceleration of gravity at sea level. The thruster efficiency is a measure for the effectiveness by which input electric power is converted to thrust power:

$$\eta_T = \frac{T^2}{2\dot{m}P_e}, \tag{1.11}$$

where $P_e=I_dV_d$ is the input electric power and I_d and V_d are the discharge current and voltage respectively. The thruster efficiency can be expressed as:

$$\eta_T = \eta_i \eta_v \eta_p, \tag{1.12}$$

where η_i is the current ratio:

$$\eta_i = \frac{I_i}{I_d}. \tag{1.13}$$

I_i Is the ion current at the thruster exit. η_u Is the voltage utilization factor defined by:

$$v_i = \sqrt{\frac{2e\eta_v V_d}{m}}, \tag{1.14}$$

where v_i is the average ion velocity at the thruster exit, *m* is the ion mass and e is the electron charge. η_v represents the effective fraction of the discharge voltage used for acceleration, which is typically smaller than V_d. η_p is the propellant utilization factor which represents the ionized fraction of the mass flow or, in other words, a measure of the efficiency with which neutrals are converted to ions:

$$\eta_p = \frac{mI_i}{e\dot{m}}. \tag{1.15}$$

Neglecting the diminishing contribution of neutrals to the thrust and using the above expression for the propellant utilization, the specific impulse can be written as:

$$Isp \approx \frac{\eta_p \mathrm{v}_i}{g}. \tag{1.16}$$

1.4.3 Hall Thruster Advantages

Hall thrusters have several advantages over other electric propulsion systems that make them attractive option for spacecraft uses. The high specific impulse compared to electrothermal thrusters, allows for significant savings in propellant or dramatic increase in satellite lifetime. Since in Hall thrusters the acceleration process takes place in a quasi-neutral plasma, it is not limited by space charge effects. Hence, current densities, and as a result thrust densities, larger than the gridded ion thruster can be obtained. As a result, the Hall thruster is much more compact than an ion thruster of a similar thrust level. Hall thrusters are easy to build and assemble because of their simple annular geometry and the use of commonly available materials, compared to the ion thruster that requires precise alignment and careful production of the acceleration grids. Additional advantages are the relatively convenient voltage and current values as compared, for example, to MPD and arcjet thrusters.

1.5 Motivation and Objectives

This work deals with the performance of low power (200-300W) Hall thrusters. A crucial problem associated with Hall thruster operation at reduced power levels is the degradation of thruster performance. Experiments with a laboratory Hall thruster described in [16] have indicated this degradation. When the operating power of a given Hall thruster configuration is reduced by lowering the discharge current its performance, namely the specific impulse and the efficiency, tends to degrade [8, 17-20]. This behavior is a result of the fact that lowering the current requires reducing the propellant flow rate thus leading to a lower propellant utilization due to the smaller chance of the diluted propellant of being ionized by impacting electrons.

The standard approach to restore the high propellant utilization when the power is reduced is to scale down the thruster size [21, 22]. However, according to a simplified analysis presented in [21], magnetic material and circuit properties limit the ability to properly implement the required scaling. Since that analysis used general assumptions and did not focus on any particular power range, a question could be asked to what extent

these magnetic limitations are relevant to the 200-300 Watts power range? To answer this question, there was a need to extend the analysis and to examine the scaling down approach by magnetic simulations of down sized thrusters. Another important problem that had to be addressed was that of the operating lifetime of down sized Hall thrusters in the power range below 300 Watts.

Due to the problems and difficulties associated with the scale down approach, a different approach is adopted in the research described in this work for Hall thrusters in the 200–300 Watts power range of trying to improve the propellant utilization of a 600 Watts thruster by modification of its configuration but without scaling it down. Two alternatives to overcome the propellant utilization problem at reduced power levels, extension of the channel length and variation of the magnetic field near the anode, were investigated experimentally.

The central aim of the research described in this work is to improve the Hall thruster performance at low power levels. The first objective is the straightforward implementation of extending the channel length in order to improve the propellant utilization at reduced power levels. Channel length variations experiments were performed with the first thruster at Soreq in the past [17, 21]. That research included three cases of channel length variations, in the range of 20-40 mm range. That work focused on the 400-700 Watts power range, although a few measurements were performed at lower power levels. The present work focuses on the 200-350 Watts. The channel length was modified by locating the anode at different positions in an elongated channel. The channel was extended that way from the original (33mm) length of the 600 Watts thruster up to a length of 52mm in five steps. The implementation of this approach necessitated a design and construction of an improved laboratory Hall thruster which is appropriate to the extended channel experiments.

The second approach that was examined in the research presented in this work is to apply a higher magnetic field near the anode in order to increase the electron density there and hence the probability of the neutrals to be ionized. However, broadening the magnetic field profile by increasing the magnetic field near the anode could spoil the focusing of the plume and result in a reduced efficiency [27]. To overcome this problem, Prof. Amnon Fruchtmann, who collaborates with Soreq on the theory of Hall thrusters, have

suggested a novel idea, to apply near the anode a magnetic field with an opposite sign to that of the field near the exit. Such a magnetic field profile has a higher gradient towards the exit, which could probably result in a better focusing of the plume, and hopefully will lead to higher thruster efficiencies. The second objective of this research work was to modify the magnetic circuit in order to attain a reversed magnetic field near the anode, to test this configuration in order to validate that it operates as a thruster and to perform preliminary characterization of the thruster performance.

Thruster operation at reduced power levels results in an increased inaccuracy in the thrust measurement, due to the reduced thrust values. Since the thrust relative error is partially a result of the thrust stand calibration process; a better calibration process directly affects the thrust measurement accuracy. Therefore, the third objective of this research was to design and build a dynamic calibration system which allows calibrating the thrust stand inside the vacuum chamber and during cryopumps and thruster operation. By allowing to perform calibrations much more frequent and close to the actual measurement time, this system was expected to improve the accuracy and, as well, reduce the uncertainties related to the conditions inside the vacuum chamber.

Clearly, this research work was motivated also by the desire to increase the overall physical understanding of the Hall thruster operation with reduced mass flow rate and to provide data that can be scaled for comparison with other Hall thrusters.

1.6 Thesis Outline

The problem of the degradation of Hall thruster performance, when a given thruster configuration is operated at reduced power levels, is addressed in chapter 2. Results of experiments performed with a Hall thruster in the 200-600W power range exhibiting such degradation are presented. Also presented in chapter 2 is an analysis of the standard approach to overcome the propellant utilization problem by scaling down the thruster and proper scaling rules are outlined. Simulations of the magnetic field distribution along the channel demonstrated that the implementation of the required scaling for thrusters in the power range below 300 Watts is indeed limited by magnetic saturation. The analysis in chapter 2 shows also that the main drawback of down sized Hall thrusters in the power

range below 300 Watts is the sharp drop in their operating lifetime compared to larger size thrusters. Chapter 3 describes the vacuum test facility, the thrust stand and the error analysis. It provides a detailed description of the thrust measurement and the calibration process. It also presents the dynamic calibration system which improved the accuracy in the thrust measurement. Chapter 4 describes the construction of the improved laboratory Hall thruster. Testing of the magnetic field of this thruster is also presented in the fourth chapter. All the experiments described in the following chapters were done at the Soreq Electric Propulsion Laboratory, using the improved laboratory model Hall thruster, described in chapter 4. Chapter 5 includes a detailed description of the thruster operation and the experiment procedures. The channel was extended from 33mm length up to 52mm in five steps. The performance for each of the lengths was measured in the power range of 200-350W at 4 voltages, and different propellant flow rates. Performance improvements were observed when the length was extended from 33mm to 40mm. However, when the channel was further extended only minor performance differences were observed. Chapter 6 describes the reversed magnetic field configuration and preliminary results of thruster performance. Chapter 7 concludes and present recommendations for future work.

Chapter 2

Analysis of the Degradation of Hall Thruster Performance at Reduced Power Levels

2.1 Experimental Results of a 600W Hall Thruster

In this section the problems concerning the degradation of the Hall thruster performance when the operating power is reduced, are discussed. The results of the performance characterization measurements of a Hall thruster for operation at a discharge voltage of 300 Volts at the 200 – 700 Watts range are presented in Figs. 2.1-2.2. The power values are obtained by multiplying the discharge current values by 300 Volts. This thruster and the following results are a part of a research which was taken at Soreq in the past. These Figures demonstrate a monotonous drop of efficiency as the power is reduced. This behavior is typical of Hall thrusters [8, 17-20]. It is explained as being a result of the drop in the efficiency of the ionization process at reduced propellant flow rates.

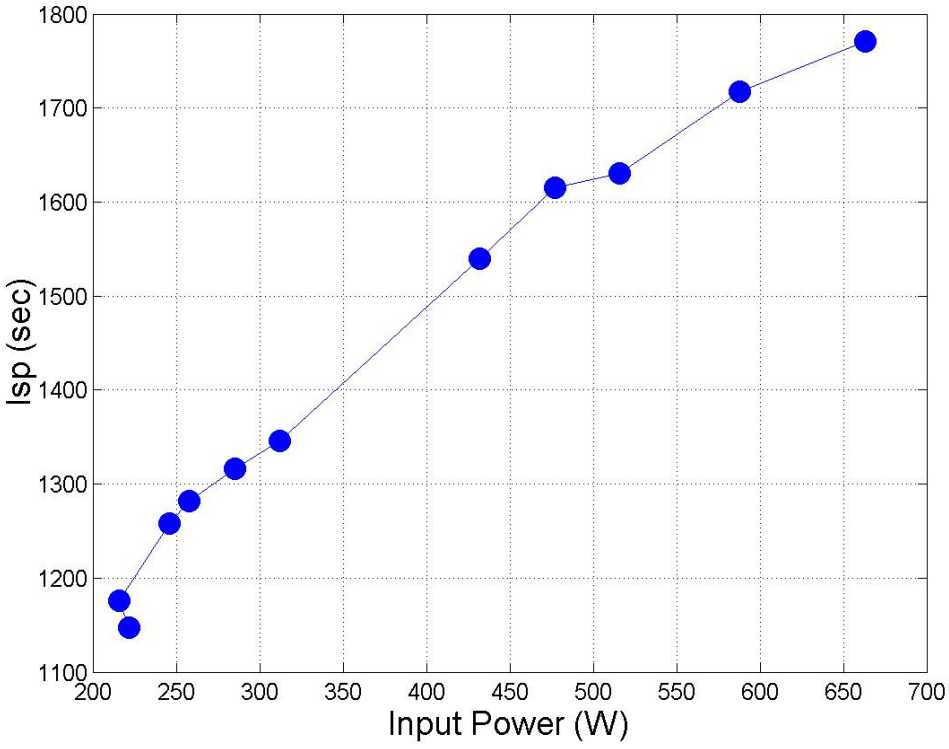

Figure 2.1: The specific impulse as a function of the electric input power at a fixed discharge voltage of 300 Volts.

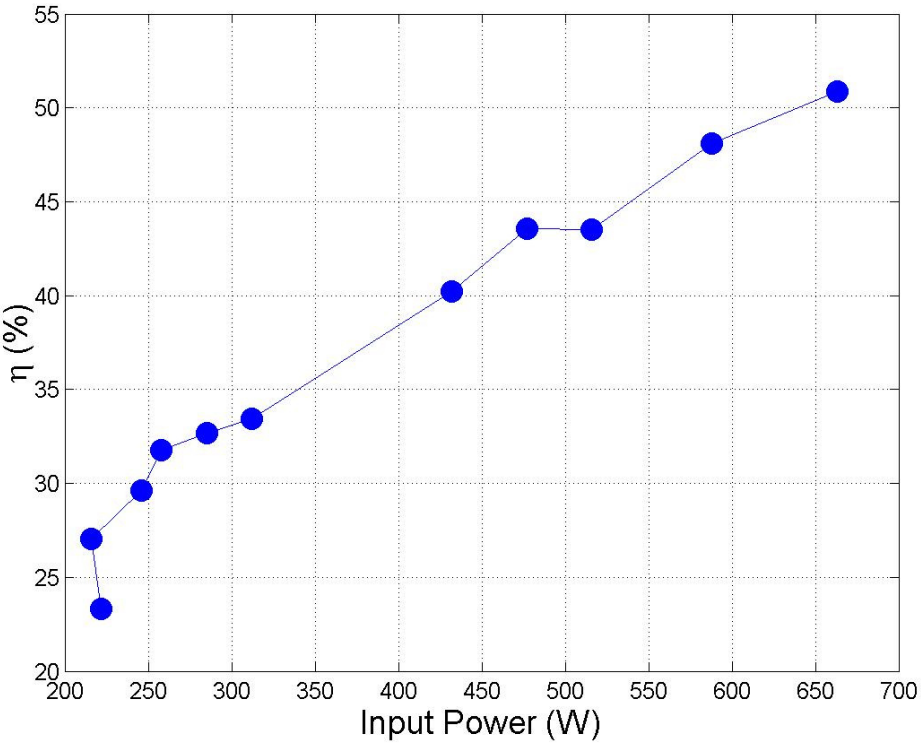

Figure 2.2: The efficiency as a function of the electric input power at a fixed discharge voltage of 300 Volts.

2.2 The Propellant Utilization Problem

When we try to operate a given thruster configuration at reduced power levels, and indeed the purpose is to keep the specific impulse and efficiency at high values, it can be implemented by reducing the discharge voltage or the discharge current. However, thruster operation at a reduced discharge voltage results in a lower ion energy and hence a decreased specific impulse, as can be seen from Equations(1.14) and(1.16). The more favorable approach is then to keep the discharge voltage fixed and to reduce the discharge current by reducing the propellant mass flow rate. However, as is demonstrated in Chapter 5 decreasing the mass flow rate at a given thruster configuration results in a reduced thruster performance.

In order to understand the behavior of the thruster while decreasing the mass flow rate let us look at the continuity equation for ions and neutrals:

$$\frac{d}{dz}(n_i \mathrm{v_i}) = -\frac{d}{dz}(n_a \mathrm{v_a}) = n_i n_a < \sigma_i \mathrm{v_e} >. \tag{2.1}$$

n_i and n_a are the ion and neutral densities respectively, v_a is the neutral velocity, σ_i is the cross-section of ionization by electron impact and v_e is the electron velocity. The right hand side of Equation (2.1) represents the ion source term. Therefore, Equation (2.1) describes also the neutral loss rate. The axial derivative of the neutral flux density could be approximated as:

$$\frac{d}{dz}(n_a v_a) \approx \frac{n_a v_a}{\lambda_i}, \tag{2.2}$$

where λ_i represents the characteristic ionization length. Using the quasi-neutrality condition, $n_i \approx n_e$, and the definition above for η_p we get for the electron density $n_e \approx \frac{\eta_p \dot{m}}{m v_i S}$, where $S = 2\pi r_m h$, is the cross sectional area of the thruster channel, r_m is the channel median and h is the channel width. Then, the characteristic ionization length can be written as:

$$\lambda_i = \frac{m v_a v_i}{\eta_p < \sigma_i v_e >} \frac{S}{\dot{m}}. \tag{2.3}$$

A criterion for a high propellant utilization is that λ_i has to be smaller compared to L, the channel length. As can be seen from Equation(2.3), even if we assume at first that η_p is not changed, when the mass flow rate is reduced, λ_i becomes larger and the propellant utilization drops. As a result, the specific impulse and the efficiency drop too (see Equations(1.12) and(1.16)).

2.3 Scale-Down Approach

As can be seen from Equation(2.3) a straightforward approach to overcome the propellant utilization problem is to scale down the channel cross-sectional area with the mass flow rate ("cross-sectional" or "radial" scaling), $S \sim \dot{m}$. In another scale down approach, also considered, all linear dimensions are scaled down by the same factor ("photographic" or "ideal" scaling). In this section, the effect of such geometrical modification on the overall thruster efficiency using a simplified analysis was examined. This analysis indicates the required changes in the magnetic field distribution in order to restore the voltage utilization and the current ratio. However, as it is shown below, these requirements are

difficult to implement due to magnetic circuit limitations. It is also shown that the scaled down approach leads to severe limitations on the expected lifetime of the reduced power thruster.

2.3.1 Cross-Sectional Scaling

Let us assume that the mass flow rate is reduced by a factor *k*, i.e., $\dot{m} \to k\dot{m}$ (*k<1)*.The main idea in the cross-sectional scaling is that the channel cross-sectional area, *S*, scales down as $\dot{m}$, $S \to kS$. Using a dimensional analysis and substituting the factor *k* into Equation(2.3), we get $\lambda_i \to \lambda_i$. As one can see, the ionization characteristic length is not changed and apparently we restore the propellant utilization.

Actually, this approach is less than ideal since the propellant utilization is affected also by recombination of ions and electrons at the channel wall, acting as a third "large body", thus reducing the propellant utilization. Since the chances of an ion to reach the wall seem to increase as the ratio *h/L* is reduced, wall recombination is expected to increase in the cross-sectional scaled-down thruster, as $h/L \to kh/L$.

2.3.2 Photographic Scaling

The wall recombination problem was maybe the reason for some people to suggest the so called "photographic" [24] or "ideal" [22] scaling, in which all linear dimensions are scaled by the same factor *k*. Then as $\dot{m} \to k\dot{m}$, $r_m \to kr_m$, $h \to kh$, $L \to kL$ and $S \to k^2 S$. From which follows that $\lambda_i \to k\lambda_i$. Therefore we get $\lambda_i/L \to \lambda_i/L$ and $h/L \to h/L$, i.e., both the ratio affecting the ionization and the ratio affecting wall recombination are conserved.

2.3.3 The "Acceleration Length"

It is important to note again that the goal in scaling down the thruster while reducing its power is to conserve the high performance of the original thruster, i.e., the specific impulse and the total thruster efficiency. As can be seen from Equations (1.13-1.19), in addition to the propellant utilization these parameters depend also on the voltage utilization, while the total efficiency depends also on the current ratio. It is our duty then

to verify the requirements in order to conserve the voltage utilization and the current ratio when the thruster is scaled down, and if these requirements can be implemented practically.

The voltage utilization and the current ratio are mainly affected by processes in the "acceleration region", the region near the thruster exit where the magnetic field is strong and as a result the electron motion towards the anode is strongly impeded and most of the voltage drop occurs. The effective length of this region, l_a, is then determined mainly by the width of the magnetic field axial distribution. That is to say, the narrower is the magnetic field distribution so is the "acceleration length", l_a.

2.3.4 Voltage Utilization

To large extent, the voltage utilization is determined by ion energy losses due to collisions with channel walls at the accelerating region. The accelerating ions thus lose part of the kinetic energy they had already acquired from the electric field (and as a result also erode the channel walls). There are at least two effects through which ion energy wall losses are affected by the accelerating region geometry. One is the "collimation angle", i.e. the angle by which the ions "see" the thruster exit plane, $\theta \sim h/l_a$. Indeed the smaller is this angle the larger is the chance of an ion to impact the walls. The second effect is the radial electric field that results from the electron pressure gradient, $E_r \approx \frac{\partial p_e}{\partial r}\frac{1}{en_e} \approx \frac{kT_e}{eh}$, which pushes the ions towards the walls. When compared to the accelerating axial electric field, estimated as $E_z \approx \frac{V_a}{l_a}$ (where the accelerating voltage, V_a, is somewhat smaller than V_d), we get:

$$\frac{E_r}{E_z} \sim \frac{kT_e}{eV_a}\frac{l_a}{h}. \tag{2.4}$$

It is clear then that in order to avoid an increase in ion energy losses due to the collimating and the electron pressure effects, and thus to conserve the voltage utilization, the “acceleration length” must scale with the width of the channel, i.e.,

$$\boxed{l_a \sim h} \tag{2.5}$$

2.3.5 Current Ratio

Since the discharge current is the sum of the ion and electron currents, we can use the quasi-neutrality condition and write the current ratio, η_i, as a function of the ratio between the electron and ion axial velocities

$$\eta_i = \frac{I_i}{I_i + I_e} = \frac{1}{1 + \frac{\mathrm{v}_e}{\mathrm{v}_i}}, \tag{2.6}$$

The axial electron velocity is related to the axial electric field through the relation:

$$\mathrm{v}_\mathrm{e} = \mu_\perp E_z \approx \mu_\perp \frac{V_a}{l_a}, \tag{2.7}$$

where $\mu_\perp$ is the electron mobility across the magnetic field. As it is quite well accepted that Hall thruster behavior is dominated by anomalous diffusion, we take for $\mu_\perp$ the Bohm mobility which goes as the inverse of the magnetic field [30],

$$\mu_\perp \sim \frac{1}{B}. \tag{2.8}$$

Using Equation(1.14) we get for the ratio of velocities:

$$\frac{\mathrm{v}_\mathrm{e}}{\mathrm{v}_\mathrm{i}} \sim \frac{\sqrt{V_d}}{B l_a}. \tag{2.9}$$

Operating at a constant voltage we see that the magnetic field strength has to scale as the inverse of the "acceleration length" in order to restore the ratio of velocities and hence the current ratio, i.e.:

$$\boxed{B \sim 1/l_a}. \tag{2.10}$$

2.3.6 Magnetic Circuit Limitations

At first sight, the implementation of the scale down procedure described above seems to enable us to reach our goal of conserving the high performance of the original thruster while reducing the input power. First, the channel geometry is scaled down (either cross-sectional or photographic scaling) in order to restore the propellant utilization. Then, there seems to be no problem in reducing also the size of the magnetic circuit in order to narrow the magnetic field distribution and accordingly the "acceleration length" and thus

to restore the voltage utilization. Finally, the coil's current should be adjusted in order to increase as required the magnetic field strength and to restore the current ratio and as a result the overall thruster efficiency. As it happens however, magnetic circuit material properties and volume constraints limit our ability to perform such a scale down without a compromise on thruster performance. In addition, as we will see, these limitations add to the burden on the already reduced operating lifetime of the scaled down thruster.

The main limitation results from magnetic saturation in the circuit core parts as their size is reduced and at the same time the required field strength increases. To demonstrate this problem we refer to a simplified magnetic circuit composed of a magnetic coil, an iron core, and pole pieces forming a gap around the accelerating region. We note again that proper scaling requires that $B \sim 1/l_a \sim 1/r_m$. From which it follows that the magnetic flux in the channel is $\Phi \approx 2\pi r_m l_a B \sim r_m$. As a result of flux conservation we can write for the magnetic field strength in the magnetic circuit core, $B_i \approx \Phi/\pi r_i^2$, where r_i is the typical core radius. Assuming that the magnetic circuit parts are scaled with the rest of the thruster, $r_i \sim r_m$, we get:

$$B_i \sim \frac{1}{r_m}. \tag{2.11}$$

That is to say, as the thruster is scaled down the field strength inside the magnetic core has to increase and eventually it will reach saturation. This problem depends on The B-H curve of the core material and hence could be more severe at the elevated temperatures during thruster operation. It leads to flux losses and distortion of the magnetic field distribution and, as a results, prevents from obtaining the required "accelerating length" and/or magnetic field strength in the channel of the scaled down thruster.

In principle, the saturation problem could be partially avoided if the cross sectional area of some of the iron core parts, those which do not directly affect the field distribution, is scaled down only as r_m or less. In this case we will have $B_i \sim$ constant inside these parts. However, this approach is limited by the available volume, especially at the thruster center, when the channel is scaled down. The problem of available volume becomes more severe when we consider also the coils. To see that let us refer again to the above mentioned simplified magnetic circuit whose equation is given by:

$$NI_c = \Phi(\Re_i + \Re_g) \ , \tag{2.12}$$

where N is the number of coil turns and I_c is the coil current. $\Re_i \approx l_i/(\mu\mu_0\pi r_i^2)$ is the iron core reluctance, and $\Re_g \approx h/(2\mu_0\pi l_a r_m)$ is the gap reluctance. Since the iron permeability $\mu >> 1$, $\Re_i$ can be neglected compared to $\Re_g$, and we get:

$$NI_c \approx \Re_g \Phi \ . \tag{2.13}$$

Since $\Phi \sim r_m$ and $\Re_g \sim \frac{1}{r_m}$, it follows that NI_c has to remain constant as the thruster is scaled down and the available volume diminishes. Trying to avoid this problem by increasing the coil current on the expense of N could result in increased power dissipation in the coils leading to a reduced overall efficiency and increased heat load problem. The increased coil current could result in additional penalty in terms of added mass and volume of the coil power supply. Another approach is to avoid the use of internal coils. However, this requires simplifying the magnetic circuit topology and would result in a compromise in the ability to control the magnetic field distribution and in particular l_a.

The dimensional analysis above has demonstrated that in general the scale down approach is eventually limited by saturation problems and volume constraints. Nevertheless, since our present interest is in 200-300 Watts thrusters, it is important to verify whether such problems are encountered already in this power range. For that purpose we used a finite-element simulation to compare the magnetic circuit of the 600 Watts thruster (r_m = 56mm) with the same magnetic circuit scaled down by a factor of $0.5^{1/2}$, which roughly corresponds to a cross-sectional scaling to a 300 Watts thruster (r_m ≈ 40mm), and by a factor of 0.5, which corresponds to an ideal scaling to a 300 Watts thruster (r_m = 28mm). As required by the dimensional analysis, the same value of Ampere-turns (NI_c) was used in all three simulation cases, corresponding to a coil current of 2A for the 600 Watts thruster. By doing so, we disregarded the volume constraints and/or dissipation problems mentioned above. A theoretical B-H curve for steel 1010 with a saturation value of ~ 18KGauss was used in the simulations. It should be noted that this curve is favorable compared to the B-H curves measured at room temperature and at 400°C with saturation values of ~ 15KGauss and ~ 13KGauss respectively [29].
The simulated magnetic field distributions along the channel median for the three cases are shown in Figure 2.3. They demonstrate the expected narrowing of the field distribution and increase in field strength as the magnetic circuit is scaled down. The

simulation results are summarized in Table 2.1. The first column shows the values of the geometrical scale factor, k, while the second one indicates the uniformity of the Ampere-turns value. The third column shows the required scale factors for the magnetic field strength. These factors have to be compared with the simulated scale factors for the magnetic field strength at the central iron rod and at the channel median, shown respectively in the last two columns together with the corresponding field values. The discrepancies between the simulated and required scale factors which increase as k becomes smaller are a result of saturation. They indicate the difficulties in obtaining the required magnetic field strength for scaled down thrusters in the 200- 300 Watts power range. In reality, with a less ideal B-H curve, and with coil volume constraints and heat load, these difficulties are expected to be much worse.

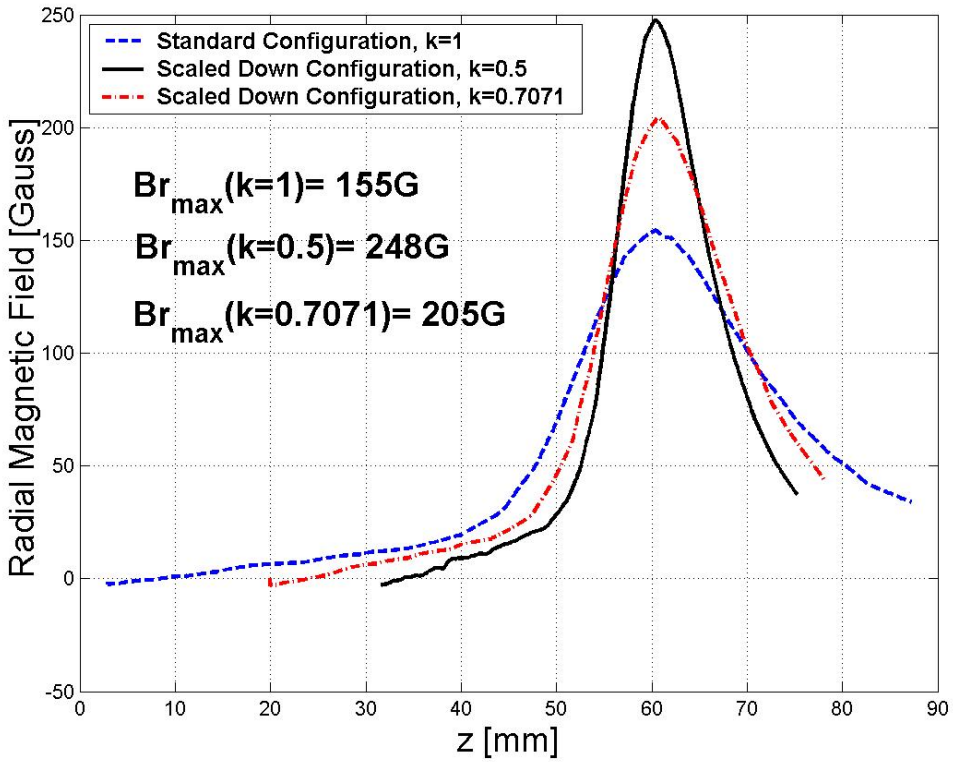

Figure 2.3: Simulated radial magnetic field along the channel axis for the original (k=1) and for two scaled-down configurations, $k=0.5^{1/2}$ and k=0.5.

Table 2.1: Required and simulated magnetic scale factors, and simulated field values, for the original and for two scaled-down magnetic circuits (all magnetic circuit parts are scaled-down by the same factor k).

Scale factor	**k**	NI_c	**Magnetic Field strength** (Required)	**Max. Bz central rod** (Sim.) **value**	**Max. Br channel median** (Sim.) **value**
Original circuit ($r_m = 56$ mm)	1	1	1	1	1
				11 kG	**155 Gauss**
Scaled circuit 1 ($r_m \approx 40$ mm)	$\frac{1}{\sqrt{2}}$	1	$\sqrt{2}$	1.35	1.32
				13.5 kG	**205 Gauss**
Scaled circuit 2 ($r_m = 28$ mm)	$\frac{1}{2}$	1	2	1.6	1.6
				16 kG	**248 Gauss**

2.4 Operating Lifetime of Down Sized Hall Thrusters

While the main advantage of electric propulsion is the very large specific impulse, electric thrusters of all kinds including Hall thrusters are known also to be characterized by their very low thrust. Since a spacecraft propulsion mission is determined by the required total velocity increment, Δv, (or the required total impulse), the low thrust of electric thrusters results in a very long operating time, in the range of hundreds or thousands of operating hours. Moreover, as it is more beneficial to use electric thrusters in large Δv missions, where the mass saving is large, the demand to extend the operating lifetime of electric thrusters can be expected to continue in the future.

In order to consider what happens to the required operating lifetime, $t^*_{life} = M_{fuel}/\dot{m}$, when the onboard power available for thruster operation is reduced, we use the expression for the thruster efficiency, Equation(1.11), and the rocket equation:

$$M_{fuel} = M_0(e^{\Delta v/gIsp} - 1) \quad , \tag{2.14}$$

where M_{fuel} is the fuel mass required to accomplish the mission and M_0 is the empty spacecraft mass, to get:

$$t^*_{life} = \frac{g^2 Isp^2}{2\eta_T}\frac{M_0}{P_e}(e^{\Delta v/gIsp} - 1) \tag{2.15}$$

As we can see, even if we succeed in obtaining the high performance of higher power thrusters, namely the specific impulse and the efficiency, the reduced onboard power tends to extend the required operating lifetime. Furthermore, even if the reduced power thruster is intended for use onboard a smaller size spacecraft, e.g., a micro-satellite; we still need to keep the same specific power, P_e/M_0, not a simple task by itself, in order not to extend the required lifetime. To summarize, the operating lifetime of future low power electric thrusters is required to be not smaller, and most probably larger, than that of present and near future higher power thrusters.

While the last paragraph deals with the required operating lifetime of reduced power thrusters, let us now try to estimate what happens to the actual operating lifetime of scaled down Hall thrusters. First, we note that the erosion of the ceramic channel walls by colliding energetic ions in the acceleration region is usually regarded as the main mechanism of thruster degradation determining the operating lifetime. Generally speaking, the channel erosion rate can be described by the following equation:

$$\frac{dh_c}{dt} = -J_{ri} f(E_{i,} \vartheta_{iw}, cer), \tag{2.16}$$

where, J_{ri} is the radial ion flux density, h_c is the ceramic wall thickness, and f is a function relating the effectiveness of erosion by the colliding ions to their kinetic energy, E_i, the angle of impact at the wall, ϑ_{iw}, and the ceramic material properties represented by the variable *cer*. Assuming that the operating conditions are practically unchanged during the mission, the thruster lifetime will be proportional to the initial channel thickness, h_{c0}, and inversely proportional to the radial ion flux density. If the magnetic field profile and strength are scaled down properly as outlined in sections 4.4 - 4.5, we can further assume the radial ion flux density to be proportional to the ion current density,

$$J_{ri} \propto J_i, \tag{2.17}$$

where the ion current density is given by:

$$J_i = \frac{I_i}{S} \approx \frac{e}{m} \eta_p \frac{\dot{m}}{S}. \tag{2.18}$$

Then we can write for the thruster lifetime:

$$t_{life} \sim \frac{h_{c0}}{J_i}, \tag{2.19}$$

This result can be used to assess how the thruster operating lifetime behaves in the two scaling cases discussed above:

"Cross-Sectional" Scaling

In this case, the channel cross-sectional area, *S,* scales as the mass flow rate:

$$S \sim \dot{m}\,, \tag{2.20}$$

and hence the initial ceramic wall thickness goes as:

$$h_{c0} \sim h \sim \sqrt{\dot{m}}\,, \tag{2.21}$$

while the ion flux:

$$J_i \sim const\,. \tag{2.22}$$

It follows that the thruster lifetime scales as:

$$t_{life} \sim \sqrt{\dot{m}}\,. \tag{2.23}$$

"Photographic" Scaling

In this case we have:

$$h_{c0} \sim h \sim \dot{m}\,, \tag{2.24}$$

and:

$$S \sim \dot{m}^2\,. \tag{2.25}$$

As a result we get for the lifetime:

$$t_{life} \sim \frac{h_{c0}}{J_i} \sim \dot{m}^2\,. \tag{2.26}$$

Noting again that at a fixed discharge voltage, $P_e \sim \dot{m}$, these results indicate that if we scale for example a 600 Watts thruster with a lifetime of 4000 hours to 300 Watts, its lifetime will be reduced to ~ 2800 hours in the "cross-sectional" case and to only 1000 hours in the "photographic" case! While this trend of lifetime reduction, especially in the "photographic" case, already is disappointing, in reality thing can be expected to be even worse. As discussed above, saturation in the scaled down magnetic circuit core could result in a compromise on the proper scaling of the magnetic field profile and strength and as a consequence in additional wall collisions and heating. Potentially increased dissipation in the coils due to the Ampere-turn limitation and the fact that the ceramic channel walls are thinner in the scaled down thruster could also contribute to the rise in

the temperature of the magnetic core and, as a result, to a further enhancement of the saturation problem.

In light of the above discussion it is maybe not surprising that operating lifetime values attributed in the literature to down sized Hall thrusters in the power range below 300 Watts are much smaller than that of larger thrusters. The Publications [31] include information on the lifetime of down sized Hall thrusters in the 200–300 Watts power range, for which we found information on lifetime. It should be emphasized that none of the lifetime values appearing in these references is a result of a lifetime test! Nevertheless, the values mentioned, 1000 – 2000 hours, are much smaller than the 3000 – 4000 hours usually attributed to a 600 Watts class thruster [31].

2.5 Scale Down Summery

The standard approach to restore the high propellant utilization when the power is reduced is to scale down the thruster size. Scaling rules for the thruster geometry and the magnetic field were outlined. However, magnetic material and circuit properties limit our ability to properly implement the required scaling. As was demonstrated by magnetic simulations, these limitations cannot be disregarded in the case of scaled down thrusters for the power range below 300 Watts. The inability to implement the required scaling leads to increased wall collisions and erosion and to increased electron current and heat dissipation. As a result, the specific impulse and the total efficiency of such a scaled down thruster tend to fall short of those of the original higher power thruster.

While their somewhat lower performance could still be regarded as acceptable, the main drawback of down sized Hall thrusters in the power range below 300 Watts is the sharp reduction in the operating lifetime compared to larger size thrusters, as demonstrated in Table 2.2. The analysis indicated a few possible reasons for this drawback. One is the thinner ceramic walls required by proper scaling. In the case of ideal scaling, the increased ion current density strongly enhances the wall erosion rate. To these we have to add the above mentioned increased wall erosion and heat dissipation associated with the magnetic limitations.

Due to the problems and difficulties associated with the scale down approach, a different approach was adopted in this research work for Hall thrusters in the 200–300 Watts

power range of trying to improve the propellant utilization of the 600 Watts thruster by modification of its configuration without scaling it down. The modifications include extending the channel length (chapter 5) and modification of the magnetic field profile (Chapter 6).

Chapter 3

Experimental Set-Up

3.1 Vacuum System

The vacuum system consists mainly of a stainless steel vacuum chamber 1.2m in diameter and 3m long, two cryogenic pumps (APD-22), each of which consists of a refrigerator and a compressor, and a mechanical pump that is placed outside the laboratory in order to minimize noise and vibrations during measurements [14]. The rotary pump is connected to the chamber with a flexible tube through a filter which prevents entrance of oil particles from the rotary pump to the vacuum chamber (Back stream). The vacuum chamber contains eight flanges, four of which serve for connections of probes and power supplies to the engine that is mounted on a thrust stand inside the chamber. A Perspex window is installed on one of the flanges in order to inspect the thruster during operation. A Schematic drawing of the vacuum facility is shown in Figure 3.1.

The pressure in the range below 10^{-3}Torr is monitored by an Ion gauge which is controlled by a multi gauge controller. When xenon is flowing in the chamber, we need to correct the indicated pressure by dividing the gauge pressure reading by 2.87, in order to get the correct pressure in the vacuum chamber. The pumping speed is such that when xenon flow of 11SCCM is established in the thruster (10SCCM in the thruster itself and 1SCCM in the cathode), the corrected pressure, as obtained by the ion gauge reading, is about of $2.1*10^{-5}$Torr. This corresponds to a pumping speed of about 7000 l/s.

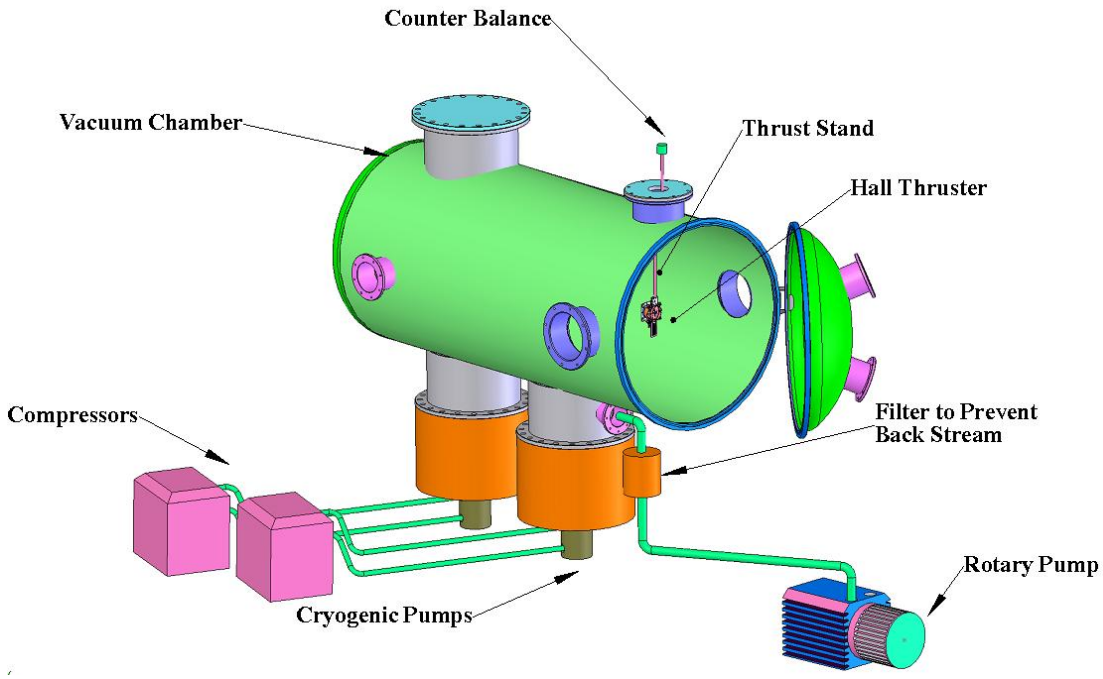

Figure 3.1: Vacuum facility schematic.

The Cryogenic pump

The cryogenic pump creates vacuum by capturing and retaining gases on very cold surfaces. It evacuates the gas in the chamber by freezing and retaining the gases from the chamber. For this reason it is ideal for creating dry, clean and high vacuum. In order to retain the pumped gases, the cryogenic surfaces in the pump must always remain below a critical temperature, or the frozen material will vaporize and the vacuum will be lost.

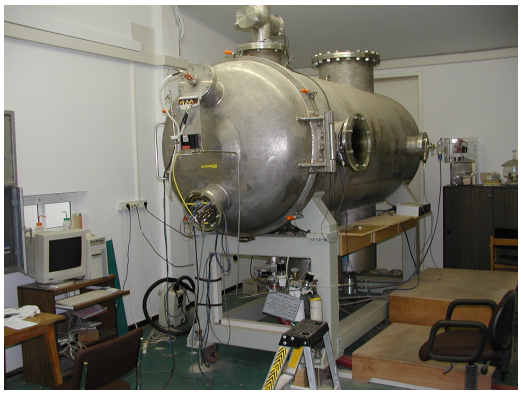

Figure 3.2: The vacuum test facility.

Mass Flow Controller

A commercial gas mass flow control and measurement system, calibrated for Xenon, is used to control and measure the propellant flow to the thruster [19]. This system includes

two Tylan FC-260 controllers (0-40sccm for the anode, 0-20sccm for the cathode). The FC-260 controller is a self-contained, closed loop control device that measures the gas mass flow rate through a flow sensor, compares this with an externally prescribed flow rate, and drives a thermal valve to keep the flow at the prescribed level. According to the manufacturer, the accuracy of this device is 1%. The anode and cathode mass flow rates are prescribed and displayed on the Tylan RO28 readout and control box. Xenon is delivered at 40psi from 25L tank using a two-stage regulator and flows through two 0.25inch diameter stainless steel tubes to the anode and cathode respectively.

3.2 Electrical Measurements

The thruster operation is performed by using several electrical sources, while the discharge current value is the electrical output which characterizes the thruster performance. Main power to the thruster (discharge voltage) is provided by a 300V – 5A DC power amplifier (Delta Electronika). Two additional supplies are used to power the cathode (only during the engine start). One to heat the filament and one to maintain the keeper current. The coils current is provided by a 30V – 5A power supply. The AC discharge current is measured using a LECROY 9304 digital oscilloscope. The DC discharge current is measured by a LEM CT-5-T Hall probe.

3.3 Thrust Measurement

3.3.1 Pendulum Type Thrust Stand

Since the Hall thruster is a propulsive device, thrust is the fundamental measurement of the thruster performance. From the thrust, mass flow rate and discharge current measurements, the specific impulse and efficiency can be computed (see Eqs.(1.10) and (1.11)). Due to the low levels of thrust, a displacement type measurement of the thrust is preferred. The thrust stand used in the experiments is a pendulum type design with a high sensitivity Lucas-Shavits inclinometer as an angle detector [32]. The thrust stand is pictured in Figure 3.3. The thrust stands displacement is directly proportional to the applied force. Because of the small angels of deflection we can assume a linear relation between the force and the angle, as is verified by the calibration.

The commercial inclinometer is used as a gravity referenced angle detector. It operates as a closed loop torque device where the torque generator current is proportional to the angular deflection. This inclinometer movement generate current that pass through a stable resistor and the voltage drop is used as the inclinometer output. The inclinometer is located on a movable plate which is mounted on an upper flange and supported by bearings. The plate is connected to an arm made of 70cm long and 16mm diameter titanium tube. The thruster is connected (electrically insulated) at the bottom of the arm by four screws. In order to reduce moments and external forces that can influence the thrust measurements all the connections to the anode, cathode, coils, and propellant feed are implemented with flexible wires and tubes which are fixed on an additional frame that is installed on the arm so that all the cables are in the same plane normal to the direction of the thrust. The wires from the inclinometer, cathode and anode are connected to the power supplies through the upper flange. Steady state location of the thruster is controlled by using a counter balance, after installing the thruster on the thrust stand and the electrical connections.

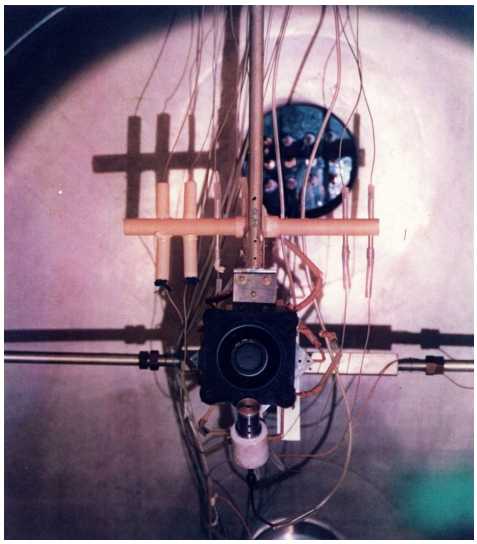

Figure 3.3: The thrust stand.

3.3.2 Thrust Stand Calibration – Manual System

The laboratory Hall thruster weight is 2.25Kg while it generates thrust of few tens of milliNewtons. Thrust stand calibration is performed with several tiny masses, between 0.2gr to 2gr, which are attached to a flexible wire while its other end passes through a 30mm diameter pulley and is connected to the thruster back plate. This set of weights enables to vary the equivalent thrust from 2mN to 35mN. The variation of the applied weight is realized by the vertical motion of the calibrating platform. In these

measurements a resolution of 0.2mN was achieved. A drawing of the manual calibration system is shown in Figure 3.4 and a typical calibration graph is pictured in Figure 3.5. The thrust stands calibration as described here can be performed only when the vacuum chamber is open. As a result its accuracy is limited by the scatter in calibrations between consecutive chamber openings which was 2-3%.

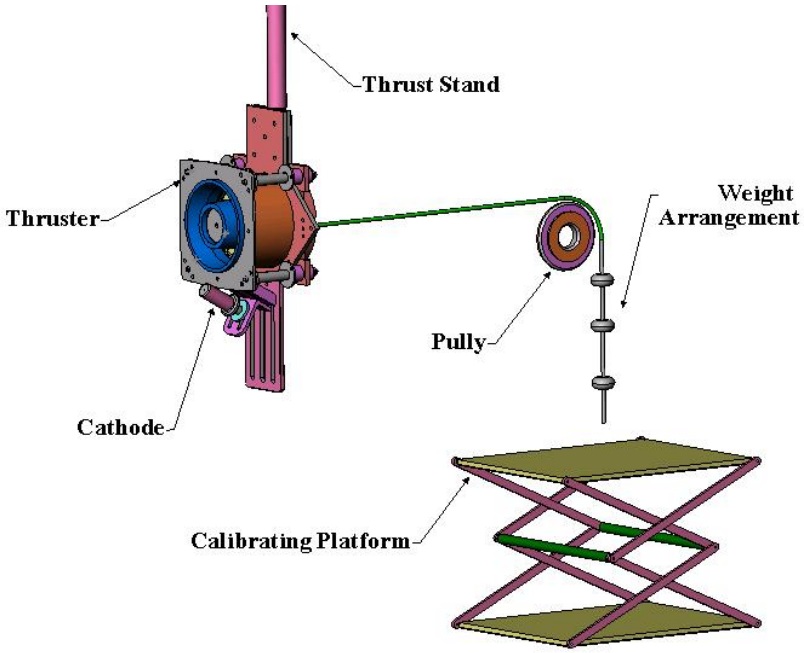

Figure 3.4: The manual calibration system scheme.

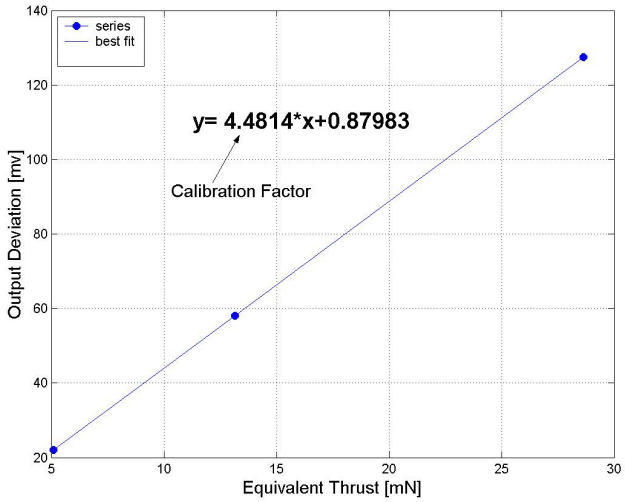

Figure 3.5: The thrust stand calibration characteristic.

The advantage of this calibration system is both in its simplicity and in knowing the equivalent thrust to a good accuracy by weighing the masses. The disadvantages of the manual calibration process described above are as follows: first, the calibration process is done under unreal typical thruster operation condition, with an open vacuum chamber without cryo-pumps, while the calibration system is not an integral part of the thrust stand. Since the cryogenic pumps operation results in a vibration of the thrust stand it is important to verify its influence on the calibration factor during the thruster operation. Second, in the calibration process, while lowering and lifting the calibration platform, the tiny masses could become wrapped with the wire; therefore, our interference is needed in order for the calibration process to be accomplished.

3.4 Dynamic Calibration Development

To improve the accuracy and, as well, to reduce uncertainties related to the conditions inside the vacuum chamber during cryopumps and thruster operation, a dynamic calibration system, which allows to calibrate the thrust-stand during cryopumps and thruster operation, was designed and built. It is assembled from five main parts: a movable platform, a 24V linear motor, pulley, a set of three ring shaped masses of 0.52gr, 0.83gr, 1.58gr, and a concentric housing. A schematic drawing of the calibration system is presented in Figures 3.6 and 3.7. The flexible wire is threaded through the masses which are placed on a concentric housing which is physically connected to the movable platform. The movable platform is controlled electrically by the linear motor. Lowering the concentric housing, causes the annular masses to be released one at a time and become suspended on the flexible wire. In this way, an equivalent thrust is obtained.

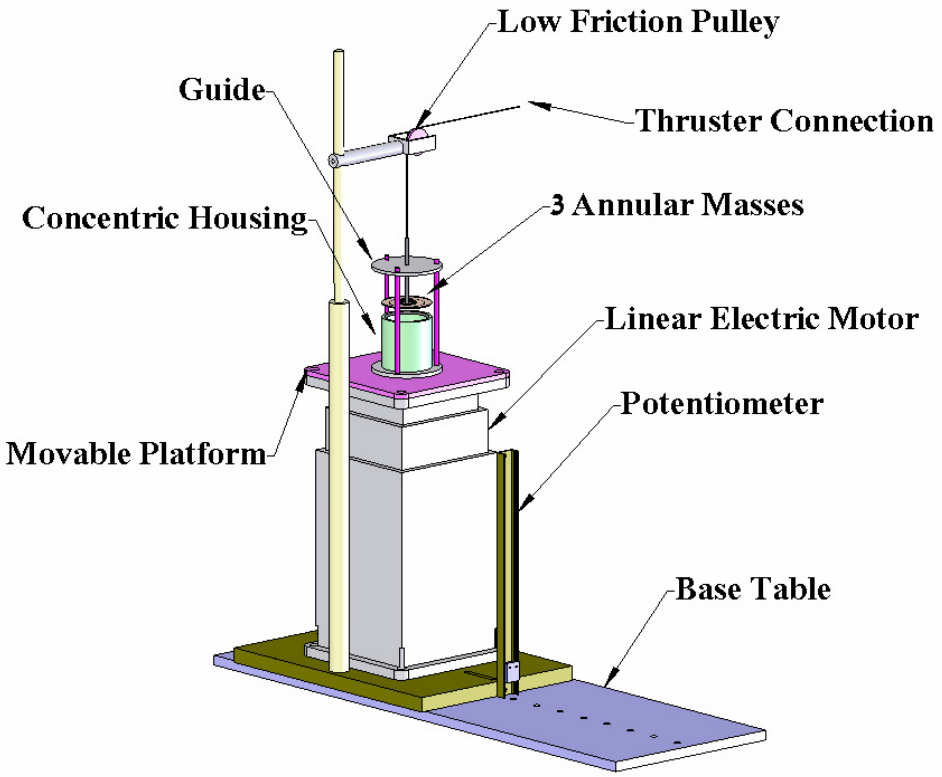

Figure 3.6: Dynamic calibration system.

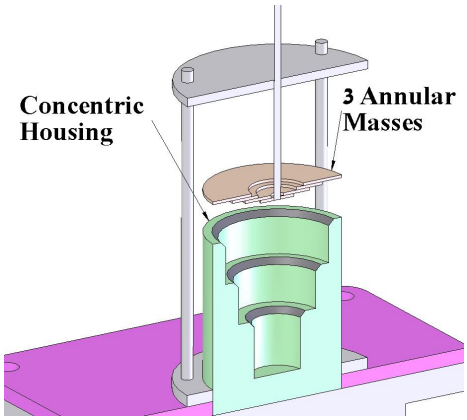

Figure 3.7: Magnified cross-section view of the annular masses and the concentric housing.

The circular Teflon guide role is to restrain the masses oscillations due to the thrust stand movement. The great advantage of this calibration system is the ability to operate it under vacuum conditions during the thruster operation, and specifically with a calibration system which is an integral part of the thrust stand. In addition, the consecutive

calibrations close to the thrust measurement time, which are enabled by this system, indeed improve the accuracy in the thrust measurement.

The dynamic calibration system was tested successfully and integrated inside the vacuum chamber. By allowing to perform frequent calibrations during thruster operation, the uncertainties were reduced and the calibration accuracy, which is characterized by the scatter between consecutive calibrations, was improved to about 0.5%. It has also shown that the cryogenic pumps have a negligible influence on the thrust measurement.

3.5 Error Analysis

The accuracy in determining the specific impulse and the efficiency is mainly affected by the relative error in the thrust measurement.

Thrust

The measured thrust is related to the output of the thrust stand by the following expression:

$$T = \frac{V_T - V_0}{\alpha}, \tag{3.1}$$

where α is the sensitivity factor in mV/mN and it is determined by the calibration of the thrust stand. V_T is the output of the thrust stand during thruster operation. V_0 is the output of the thrust stand while the engine is not operated, and the measurement process is as follows. As the thruster and the thrust stand are both in a thermal steady state, about 60 minutes from starts, and the dynamic calibration was performed, V_T is measured. Then, the thruster and the mass flow controller are turned off and after about 10 seconds (roughly the time it takes the pendulum thrust stand oscillations to decay) the inclinometer output is read. An accumulated experience has shown that in this specific time, the thrust stand drift due to cooling is negligible. So, in this case we are limited only by the resolution of the DVM connected to the inclinometer output. We assume then that the uncertainty of V_0 and V_T is about ±0.5mV for each.

From Eq. (3.1) we get the expression for the thrust measurement error:

$$\Delta T^2 \approx \left[\frac{\partial T}{\partial \alpha}\Delta\alpha\right]^2 + \left[\frac{\partial T}{\partial V_T}\Delta V_T\right]^2 + \left[\frac{\partial T}{\partial V_0}\Delta V_0\right]^2, \tag{3.2}$$

from which follows that:

$$\frac{\Delta T}{T} \approx \sqrt{\left[\frac{\Delta \alpha}{\alpha}\right]^2 + \left[\frac{\Delta V_T + \Delta V_0}{\alpha T}\right]^2} \,. \tag{3.3}$$

$\Delta\alpha$ is taken as the statistical scattering of the sensitivity factor between frequent calibrations. ΔV_T and ΔV_0 are the errors in the thrust and the zero thrust measurements which is determined by the Voltmeter resolution, which as mentioned above is ±0.5mV. The relative error in the calibration as estimated from the scatter in frequent calibrations, in the manual system is ~2.5%. Using a typical sensitivity value of 4.5mV/mN, we get

$$\frac{\Delta T}{T} \approx \sqrt{0.025^2 + \left[\frac{0.22}{T}\right]^2} \,. \tag{3.4}$$

As can be seen, as the thrust level is reduced the relative error is increased because of the second term in Eq. (3.4). The relative error in the thrust range of 10mN-20mN, by using the manual system was between 2.7% (20mN) to 3.3% (10mN) is. The dynamic calibration system, which has an accuracy of 0.5%, improved the relative error in the thrust measurement, in the range of 1.2% to 2.3%.

Mass flow Rate

During the thruster operation, the vacuum background pressure is increased due to the propellant mass flow from the thruster. The background gas which consists of Xenon atoms can enter the thruster through the exit and serve as an addition to the propellant entering the thruster through the anode and thus must be taken into account properly. Under the condition of free molecular flow, this flow of the background gas is random [15]. Applying the analysis presented in [14, 19], to our vacuum system, one can get that the effective mass flow rate due to the vacuum background pressure adds less than 2% to the measured thruster mass flow rate.

The actual mass flow through thruster can be regarded then as composed of two terms:

$$\dot{m}_{total} = \dot{m} + \dot{m}_b \,, \tag{3.5}$$

where, $\dot{m}$ is the mass flow through the anode and $\dot{m}_b$ is the additional mass flow through the thruster exit due to the background pressure. The relative error in the total mass flow rate is:

$$\frac{\Delta \dot{m}_{total}}{\dot{m}_{total}} \approx \sqrt{\left[\frac{\Delta \dot{m}}{\dot{m}}\right]^2 \dot{m}^2 + \left[\frac{\Delta \dot{m}_b}{\dot{m}_b}\right]^2 \dot{m}_b{}^2} \frac{1}{\dot{m}_{total}}. \tag{3.6}$$

According to the manufacturer, the uncertainty in the mass flow controller is, $\Delta \dot{m} / \dot{m} \approx 1\%$. While taking $\dot{m} = 0.96\,\text{mg/s}$, background pressure of $2.1*10^{-5}$Torr, the calculated mass flow rates due to the backflow pressure (2%) is 0.018mg/s. Since the background mass flow rate is calculated by using a number of assumptions, its uncertainty can be taken as 100% [19]. Therefore, the relative error in the total mass flow rate is a little more than 2%.

Input Power

The relative error in the input power is a result of the contributions of the discharge current and the discharge voltage accuracies:

$$\frac{\Delta P_e}{P_e} < 0.5\%. \tag{3.7}$$

Specific Impulse

The thrust and the mass flow rate are measured independently, so the error in the specific impulse is composed of the thrust and mass flow inaccuracies:

$$\Delta Isp \approx \sqrt{\left[\frac{\partial Isp}{\partial T}\Delta T\right]^2 + \left[\frac{\partial Isp}{\partial \dot{m}_{total}}\Delta \dot{m}_{total}\right]^2}. \tag{3.8}$$

Taking the derivatives, the specific impulse relative error is,

$$\frac{\Delta Isp}{Isp} \approx \sqrt{\left[\frac{\Delta T}{T}\right]^2 + \left[\frac{\Delta \dot{m}_{total}}{\dot{m}_{total}}\right]^2}. \tag{3.9}$$

By using Equation (3.9) the relative error in the specific impulse, with the manual calibration system, in the thrust range of 10-20mN is between 3.4% and 3.9%. By using the dynamic calibration system the results were improved to $2.3\% \le \frac{\Delta Isp}{Isp} \le 3\%$.

Thruster Efficiency

The thruster efficiency (see Eq. (1.11)) relative error is expressed as follows:

$$\frac{\Delta\eta_T}{\eta_T} \approx \sqrt{4\left[\frac{\Delta T}{T}\right]^2 + \left[\frac{\Delta \dot{m}_{total}}{\dot{m}_{total}}\right]^2 + \left[\frac{\Delta p_e}{p_e}\right]^2} \,. \tag{3.10}$$

From which it follows that in the thrust range of 10-20mN, before the calibration improvement the relative error in the efficiency was between 5.8% and 7%. By using the dynamic calibration we get: $3.1\% \le \frac{\Delta\eta_T}{\eta_T} \le 5\%$

Chapter 4

Construction of an Improved Laboratory Model Hall Thruster

An improved laboratory model Hall thruster, SLM-2, was constructed and operated in the electric propulsion laboratory at Soreq. SLM–2 design is based on the SLM–1 configuration which was designed, constructed and operated at Soreq in the past [22]. The main improvement in SLM-2 was the possibility to operate the thruster with a longer channel. In addition, the mechanical assembly of the magnetic circuit parts was improved based on the experience with SLM-1. In order to study and optimize the magnetic design, a finite element software package was used to model the magnetic circuit and simulate the field distribution. In addition, the magnetic field distribution was mapped with a Gaussmeter, demonstrating a very good agreement with the simulation field distribution.

4.1 Thruster Description

The Laboratory model SLM–2 measures 104x104x66mm and has a mass of 2.25Kg, including the mass of the cathode. The thruster is pictured in Figure 4.1. It consists of four main parts: insulating channel, magnetic circuit, anode and cathode. The design of this thruster is modular. This enables to replace, relatively easy, parts of different shapes, dimensions or materials. The magnetic circuit and the discharge chamber are 12mm longer than the previous thruster (SLM -1) in order to extend the range of available channel length up to 52mm, measured from the front surface of the anode to the channel exit.

Figure 4.1: The laboratory model Hall thruster

The insulating channel, where the ionization and acceleration take place, has to be made of an electrically insulating material which has to sustain a temperature of a few hundreds degrees. The choice of ceramic for space propulsion requires sufficient mechanical strength to survive the launch environment, and good thermal shock resistance to survive startups and shutdowns. It has an important role in electrically insulating the plasma from the iron parts which combine the magnetic circuit. Typically in Hall thrusters, the channel is made of Boron Nitride ceramic (BN), an insulating material which has a maximum operating temperature of 1800^{0}C [39]. In addition, BN has a good thermal conductivity of 27 (W/m/K) and a low thermal expansion coefficient $2.95*10^{-6}$ ($1/^{0}$C), both properties contributing to a low thermal stresses. This material can break easily and is hard to machine.

The anode has a second role as the distributor of the propellant in the annular channel. The propellant is fed from a narrow pipe through the back of the anode to an annular chamber, from which it passes through an annular narrow slot to a second annular chamber. The propellant leaves this chamber and emerges to the channel through 24 small holes (d=0.2mm) at the front of the anode, arranged in two circles of 12 equally spaced holes each. The purpose of this structure is to enhance the equal distribution of the propellant and to prevent azimuthal inhomogeneities. The anode is fabricated from a heat and corrosion resistance stainless steel which is nonmagnetic in order not to affect the magnetic field distribution. The design of the magnetic circuit is modular in order to be able to modify the magnetic configuration. The thruster cross-section is drawn in Figure 4.2 and Table 4.1 presents a list of the thruster parts.

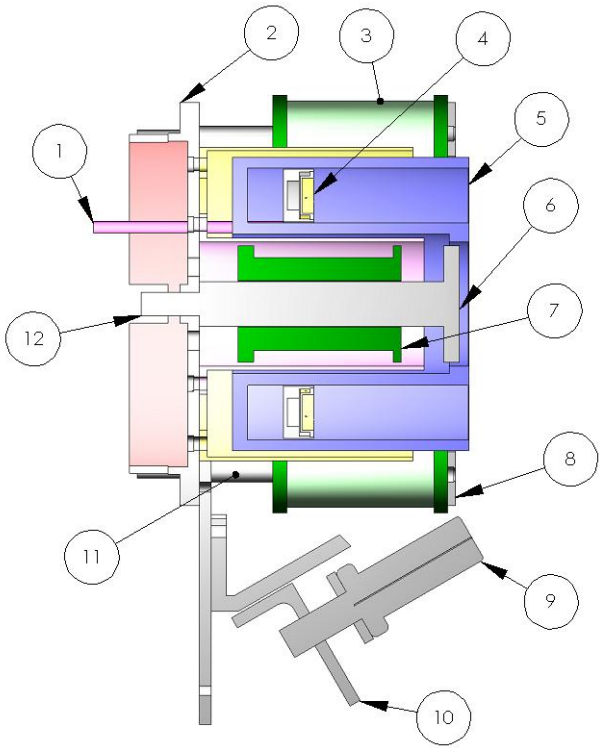

Figure 4.2: A Cross-section of a typical Hall thruster.

Table 4.1: List of the thruster parts.

Item Num.	Part Name
1	Gas flow
2	Back plate
3	External coil
4	Anode
5	Channel
6	Internal pole
7	Internal coil
8	External pole
9	Cathode
10	Cathode holder
11	External rod
12	Internal rod

Except for the internal coil holder which was fabricated from a nonmagnetic stainless steel, all other parts were machined from low carbon 1010 steel and then thermally annealed. The coil wires have to sustain the heat load from both the Ohmic dissipation

due to the current flowing through them and from the thruster body. The heated wires must also have a minimal outgasing under vacuum conditions. In addition, in order to contain the required number of turns in a limited volume, the wire insulation has to be thin enough. The electric wires used in the SLM-2 coils are 0.6mm copper with Kapton insulation.

The hollow cathode is one of the main sub-elements of the design of Hall thrusters. The cathode is pictured in Figure 4.3. The flow of the electrons emitted by the cathode is used on one hand to supply the discharge in the channel of the thruster and on the other hand to electrically neutralize the accelerated ions emerging from the thruster. The body of the hollow cathode is a tubular device with a helical emitter/heater made of porousive Tungsten impregnated with a low work function material. Current through the heater increases the temperature up to thermionic emission temperature and cause to electrons emission. By biasing an external positive electrode (keeper) that serves to accelerate the electrons, and regulating the gas flow, the source provides an electron current through a small orifice of 1mm diameter. The cathode flow rate is typically ten percent or less of the anode flow rate. The cathode steady state power consumption is low, generally on the order of 0-50W. Once the discharge is ignited, the heater and the keeper are switched-off and the plasma is maintained thanks to positive ion bombardment onto the insert surface. If the thruster is shut down or the plasma discharge goes out for any reason, the cathode discharge usually goes down as well.

Figure 4.3: The hollow cathode.

Propellant

Xenon is the propellant generally used in closed drift thrusters and the reasons for this choice are the same for gridded and Hall thrusters: First, xenon is an inert gas and therefore minimizes environmental contaminations. Second, Xenon has a low

ionization energy (12.1ev) per unit propellant mass due to a high atomic weight (131.29 amu). Third, due to a high density at relatively low tank pressure, it results in a compact tank mass. These characteristics tend to make Xenon the preferred propellant, despite its high cost.

4.2 The Magnetic Circuit

In order to study and optimize the magnetic circuit design, two different finite-element software's packages, 2-D and 3-D, were used to model the magnetic circuit and simulate the field distribution inside the iron parts and at the volume of the discharge chamber. The magnetic field distribution of the SLM-2 was mapped by a 2-axis Hall probe and the results were compared to the simulations.

4.2.1 Magnetic Circuit Design

The design of the magnetic circuit is important for the successful operation of a Hall thruster, as the magnetic field distribution determines to large extent its performance. The efficiency of the ionization and acceleration process is affected by the distribution of the magnetic field. In the Hall thruster the magnetic field traps the electrons that emitted from the external hollow cathode in an azimuthally path and prevents them from reaching the anode while the specific magnetic profile increase the electron–neutral collision frequency. The magnetic field affects also the divergence of the plasma jet.

The magnetic circuit length is 66mm, measured from the back plate to the thrusters exit plane. The magnetic circuit is fabricated from a low carbon steel 1010 which is high permeability material ($\mu \approx 5000$) and have a saturation induction of ~15KGauss. The long magnetic circuit allows to extend the effective channel length by changing the position of the anode up to 52mm. Several stainless steel spacers mounted between the channel and the anode are used locate the anode at a desired location.

The magnetic circuit is composed of five main parts as can be seen from: back plate, four external and one internal core rods, internal and external poles and screens, and four external and one internal coils. While in a flight model thruster it is preferred to make the

back plate, the internal core rod and the screens from one piece, in our laboratory thruster they are different parts which can be replaced by others with different dimensions.

In order to release the strains in the iron parts due to the machining process, they are thermally treated including 3 hours of heating to a temperature of 900^0C in hydrogen and then fast cooling at a rate of 90^0C per hour.

The coil wires are made of copper with Kapton insulation. The diameter of the conductor is 0.6mm while the thickness of the insulator is 0.13mm. This wire can sustain a temperature of more than 260^0c without outgasing.

4.2.2 Magnetic Field Simulation

Figure 4.4 shows a 2-D axisymmetric model of the magnetic circuit and the resulted field lines, in WB (Tesla=WB/m^2). The details of the magnetic circuit, the material properties and the current through the coils are inputs of the magnetic field code. We neglect the possible effect of the plasma current on the total magnetic induction. Once such a model is constructed, it is relatively easy to investigate the effect of varying the coils current or to change geometrical features such as the thickness of the poles or the length of the screens, in order to obtain a desired field distribution. The contours represent the magnetic field lines. The electric equipotentials roughly follow the shapes of the magnetic field lines as explained in chapter 1. Such a field distribution with $dB_r/dz>0$ has a tendency to focus the ions and to keep them away from the channel walls.

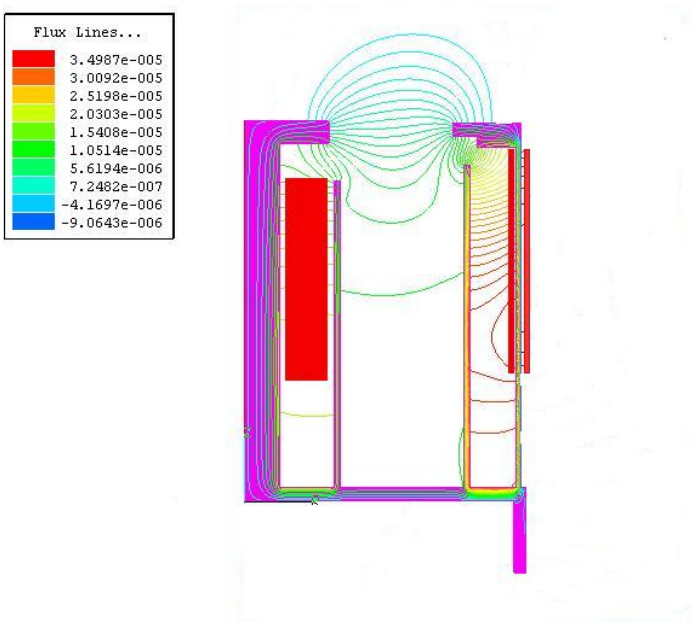

Figure 4.4: A 2-D axisymmetric finite element model of the magnetic circuit. The contours represent the magnetic field lines. The equipotentials roughly follows the magnetic field lines. The units are in WB. [10^4G=WB/m^2]

3D Magnetic Field Simulation

Since the Hall thruster is only approximately axisymmetric, a 3-D finite-element software package was used for one configuration test case. In order to verify the 2-D simulation results, the 3-D magnetic simulation was done with COSMOSEMS software which is a field simulator for low frequency electromagnetic and electromechanical applications. The simulation is based on the finite element method that solves Maxwell equations in thousands of tiny elements which describes the model. The components of the magnetic circuits were drawn and meshed using the modeling software. For simplicity, and reduction in the calculation power resources a quarter of the magnetic circuit was simulated. The B-H curve which was used in the simulation was attained from measurements performed at Rafael/Manor [29]. The materials of the magnetic parts and the coils current and the number of turns are an input values. It is important to mention that the 3-D simulation was also helpful in examining the magnetic flux distribution inside the iron parts. The simulation results for the case when the coil current is 2A are plotted in Figure 4.5. There is a good agreement between the 2-D and 3-D simulations,.

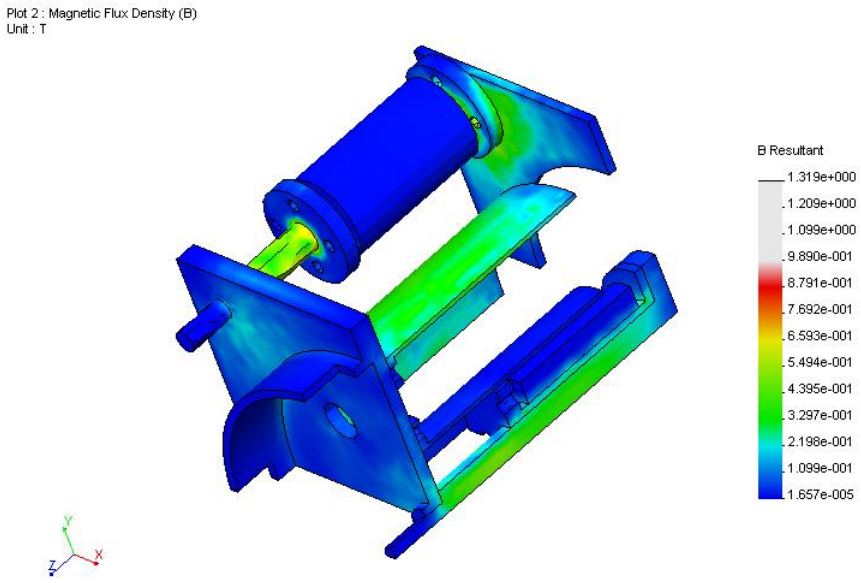

Figure 4.5: Simulation of the magnetic field strength in the magnetic circuit parts.

As can be seen from Figure 4.5, the highest magnetic field strength of ~13KGauss is obtained inside the internal rod. The external rods and the screens reached a maximum magnetic field of ~5KGauss.

4.2.3 Magnetic Field Testing

In order to actually verify the finite element simulation results, the strength and profile of the magnetic field was measured by a F.W Bell 9900 digital Gauss-meter, using a YOA-99 two-axis Hall probe which allows measuring the radial and axial components of the magnetic field simultaneously. The magnetic field test set up is pictured in Figure 4.6.

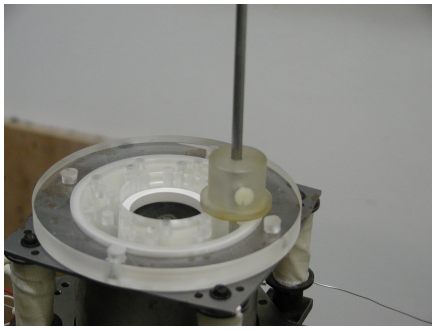

Figure 4.6: A set-up to measure the profile of the radial and axial magnetic field inside the channel. An annular disk with holes was built to hold the Gauss-meter probe parallel to the thruster axis.

In order to place the probe in a specific point (r, θ, z) inside the channel relative to the symmetry axis, a circular disk made of Perspex was fabricated and mounted on the

thruster at the exit plane. The disk was made of transparent material in order to be able to observe the probe location along the channel. 24 holes were drilled in the Perspex disk, placed along three diameters, one in the median (28 mm) and the two others near the internal and external channel walls. Probe sliding through different holes and positioning it at different axial locations enables to map the radial and axial magnetic field ($Br(r,\theta,z)$, $B_z(r,\theta,z)$).

A comparison between the measured and simulated magnetic field distributions at the channel median is presented in Figure 4.7. The maximum magnetic field value obtained from the finite element simulation is ~5% higher than the measured magnetic field maximum. As can be seen, the field distribution is such that nearly no radial field is present close to the anode, with an increasing distribution peaking at the exit plane. Moreover, the axial component of the magnetic field, B_z, is much smaller than the radial one along the whole channel. This shaping of the magnetic field helps minimize ion losses to the channel walls and increase thruster's performance. By minimizing ion impact in the ceramic wall, erosion is limited and ions are not wasted, thereby increasing the performance and life time of the thruster. In Figure 4.7, the measured maximal value of the radial magnetic field was about 5% lower than the simulated one for the same coils current of 2A. This result are much better than the measurements which were taken with the SLM-1 in [14], where a 15% lower measured B_r was obtained than the simulation value. I tend to attribute this improvement mainly to the modified mechanical assembly of the SLM-2.

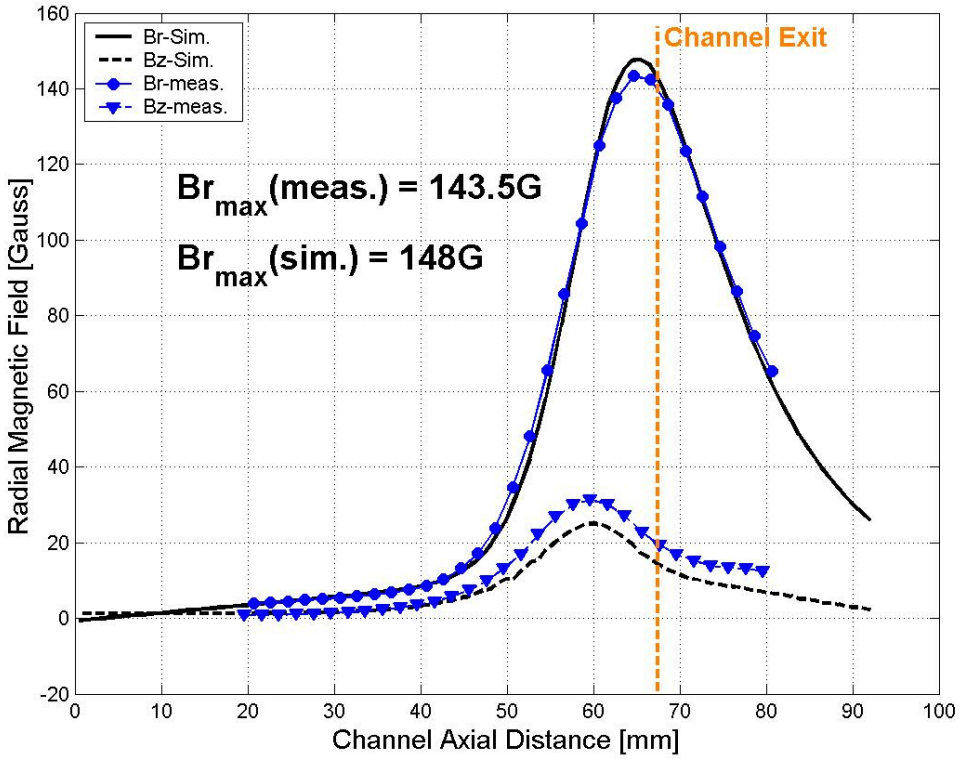

Figure 4.7: Measured and simulated results of the axial and radial magnetic field distribution at the channel median. The results were taken with I_c=2A.

Chapter 5

Parametric Investigation of the Dependence of Thruster Performance on the Channel Length at Low Power Operation

5.1 Introduction

This chapter describes an experimental investigation of the improvement potential of Hall thruster performance at reduced power levels by channel length extension. The channel length of the laboratory model Hall thruster, SLM-2, was effectively changed by locating the anode at five different axial positions inside the channel. The thruster performance for each of the five lengths was measured at the 200-350 Watts power range for various voltages and propellant flow rates. Performance improvements were observed when the channel was extended from the original length (33mm) up to the 40mm. However, when the channel was further extended up to 52mm, the changes in the thruster performances were very small.

As described and analyzed in chapter 2, when the operating power of a given Hall thruster configuration is reduced by lowering the discharge current (and keeping the voltage fixed) its performance, namely the specific impulse and the efficiency, tends to degrade (the alternative approach of lowering the voltage is even worse as it directly reduces the specific impulse). This behavior is a result of the fact that lowering the current requires a reduction of the propellant flow rate leading to a lower propellant utilization due to the smaller chance of the diluted propellant of being ionized by impacting electrons.

Due to the problems and difficulties associated with the scale down approach, as demonstrated in chapter 2, a different approach for Hall thrusters in the 200–350 Watts power range, to improve the propellant utilization of the 600 Watts thruster by modification of its configuration without scaling it down, was adopted in this research work. This approach has the advantage of avoiding the short reduction in the operating

lifetime, and maybe even extending it, and as well, shortening of the development process by building on the experience with the 600W thruster. A straightforward configuration modification is to extend the length of the thruster channel. According to the analysis in chapter 2, the channel length, L, must be longer than the characteristic ionization length, λ_i, in order to obtain good ionization efficiency. Therefore, extending the length of the channel can serve as an alternative to the geometrical scaling approach as a mean to overcome the propellant utilization problem when the mass flow rate is reduced.

As can be deduced from the analysis in chapter 2, since the channel width, h, is unchanged, the magnetic circuit dimensions and as well B or NI_c need not to be changed. As a result we are not limited by saturation and problems of available space. According to that analysis, the ceramic wall initial width, h_{c0}, and the channel cross-sectional area, S, are unchanged. Therefore, the ion current density goes as:

$$J_i \sim \frac{\dot{m}}{S} \sim \dot{m},$$

and as a result, the thruster lifetime, which as mentioned in Chapter 2 is limited mainly by channel wall erosion, even tends to increase:

$$t_{life} \approx \frac{h_{c0}}{J_i} \sim \frac{1}{\dot{m}}.$$

As one can see, the thruster operation at reduced mass flow rates and input power levels could result in an improved lifetime.

5.2 The channel Extension

Channel length variations experiments were performed at Soreq in the past [16, 17, 21] with the first laboratory thruster, SLM-1. That research included three cases of channel length variations, in the range of 20-40 mm range. That work focused on the 400-700 Watts power range, although a few measurements were performed at lower power levels. The present work focused on the 200-350 Watts power range and tested five channel length configurations between 33mm (original 600W length) and 52mm. As described in chapter 4, a new laboratory model Hall thruster, SLM-2, was designed and built on the basis of SLM-1, but which allowed for a wider range of channel lengths. In addition, the mechanical design of the magnetic circuit was improved based on the experience with the

first laboratory thruster. The desire to test a wider range of channel lengths came out of the assumption that at even lower power levels there could be an advantage to go to even larger lengths.

The channel cross-section and the movable anode are presented in Figure 5.1. The channel length was modified by locating the anode at different positions, by using three spacers, made of stainless steel, for each thruster configuration.

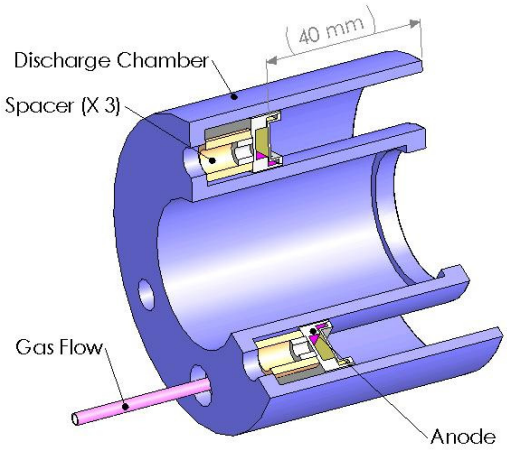

Figure 5.1: Assembly drawing of the movable anode and the ceramic channel.

5.3 Thruster Operation

In this section the general operation procedure of the SLM-2 will be briefly reviewed. Once the vacuum chamber is pumped to ~10^{-6}Torr level, Xenon gas at a mass flow of ~ 0.2 mg/s is flown through the cathode for half an hour in order to fill the lines connecting the Xenon tank to the cathode and to purge residual air. Then, the outgasing process can begin. The cathode emitter is very sensitive to moisture and oxygen. Therefore it is important to condition the cathode in order not to damage it. The outgasing process includes applying a current of 8A through the heater for ten minutes and then another 50 minuets with a current of 12A. As the cathode outgasing process is done, the thruster ignition process can be started. First, the anode mass flow rate is initiated at the desired value and the coils current is fixed on ~ 1.5A, and the cathode heating current is increased to 22A. Next, the cathode keeper power supply is turned on, and regulated to a voltage of ~50V, and the anode voltage is adjusted to 300 Volts. From this moment, it takes nearly two minuets until the cathode and the thruster ignition. Once the cathode starts, the cathode heater and keeper can be turned off, as the cathode will be self heating

during thruster operation. The cathode purging and outgasing processes are performed only at the first attempt to operate the thruster after the cryo-pumps are turned on. The following thruster operations begin with the ignition process described above.

During the first hour of operation the thruster and the thrust stand are warmed up until reaching a thermally steady state condition. It is important to note that no measurement is taken until the thrust stand reaches this mode. In addition, after the first hour of thruster operation it tends to run better in this warmed up state with smaller discharge current oscillations. These current oscillations mainly exist close to the thruster start, due to outgasing of the thruster surfaces particularly the dielectric walls which absorb moisture when not kept under vacuum. A picture of the SLM-2 during operation is presented in Figure 5.2.

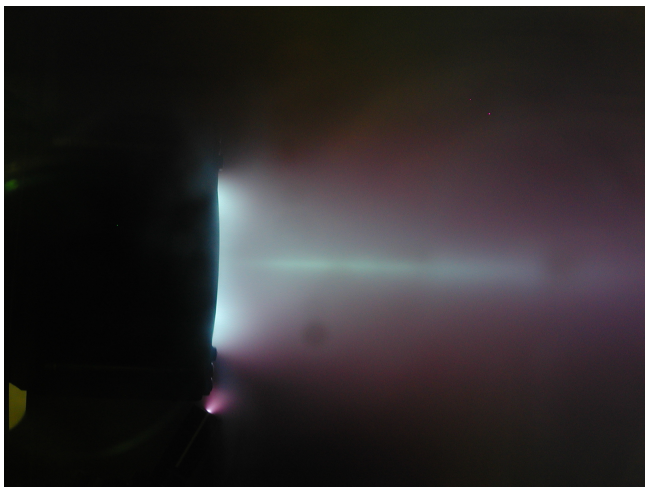

Figure 5.2: The SLM-2 Hall thruster during operation.

The commercial hollow cathode used in the experiments described in this work was designed to operate with a minimum discharge current of 1.3A in a self heating mode. Even though, it was possible to operate a new cathode in this mode at lower discharge current values for some time. However, after a few hours of thruster operation, the cathode operation and as a result also the thruster operation became unstable. In order to keep the cathode in a stable operation it was needed to enhance the electron current by applying additional heating power to the cathode heater/emitter of about 10W, in an input power of 300W and about 30W in an input power of 200W. One explanation to this instability problem is the inability of the cathode to supply enough current in a fixed mass flow rate and discharge voltage, due to contamination of the heater /emitter by the iron

atoms which are sputtered from the external pole or from the chamber walls by energetic ions. These iron atoms supposedly penetrated into the cathode through the orifice and covered the emitter surface. The iron coating could prevent or reduce electron emission. This issue was partially solved by covering the exposed iron components of the thruster with a layer of Boron Nitride.

5.4 Measurement Process

Once the thruster is started, an inspection of the plume is made in order to verify the symmetry of the plume. The discharge voltage and mass flow rate are fixed at the desired working point. Then the coils current is adjusted in order to minimize the discharge current which will generally maximize the thruster efficiency. Together with the voltage and mass flow rate, this value of the coils current for which the discharge current is minimal defines the working point. Coils current below this value results in increased axial electron mobility as the magnetic field strength is decreased and the result is increased axial electron current and hence increased total discharge current. The case of higher coils current results in an increased discharge current, I_d, despite the decreased axial electron mobility. The higher discharge current is associated with the appearance of current and voltage oscillations at frequencies of tens of kilohertz whose amplitude increases with I_c. One possible explanation for this behavior is that the axial electron current is too low to sustain at steady-state the ionization of neutral flux from the anode [17, 23]. A typical graph of the discharge current as a function of the coils current is presented in Figure 5.3.

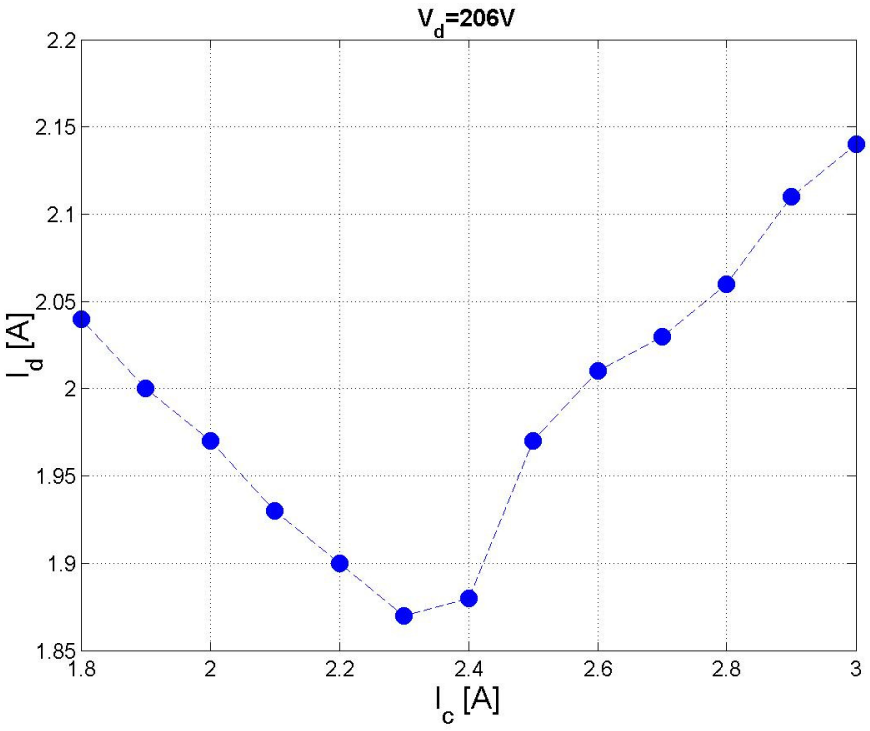

Figure 5.3: A typical graph of the thruster discharge current as a function of the coils current, obtained at a discharge voltage of 250V and xenon flow rate of 1.04mg/s. The working point is usually at the minimum discharge current.

As the thruster and the thrust stand are both in a thermal steady state, about 60 minutes from starts, in a constant mass flow and discharge voltage, the dynamic calibration is performed, during thruster operation. Then, the thruster and the mass flow controller are turned off in order to read the inclinometer output, while the thruster is not operated. Once this process is accomplished, the thruster performance, namely thrust, specific impulse and efficiency are calculated, using the Equations in chapter 2. This measurement process is repeated with different discharge voltages and mass flow rates.

5.5 Results

Measurements were performed at the discharge voltage range of 250-330 Volt, Xenon mass flow range of 0.8-2mg/s, input power range of 200W-600W, and coil current of 1-3A. At each operating point, which is characterized by a fixed discharge voltage, coils current and mass flow rate, the discharge current and thrust were measured, from which specific impulse and efficiency were deduced. Five different channel length configurations were investigated: 33, 37, 40, 45, 52mm. Before each channel length

measurement set, the anode was cleaned and located at the desired length. The anode was cleaned in order to minimize the effect of sputtered material from the vacuum chamber walls on the results of the measurements. The thruster was operated also at ~150 Watts (V_d=200-300V). However, after a few minutes the thruster operation became unstable, and thrust measurements were not performed at these points.

5.5.1 The Dependence on Voltage and Mass Flow Rate

The thruster performance results for the 33mm channel length are presented in Figures 5.3-5.6. Shown in Figure 5.3 is the measured discharge current versus the mass flow rate for different values of the discharge voltage. The corresponding thrust, specific impulse and efficiency are shown in Figures 5.4-5.6. Figures 5.7-5.22 demonstrate the discharge current, thrust, specific impulse and efficiency for channel lengths of 37, 40, 45, 52mm. As can be seen in the graphs, a dashed line connects the discrete points which represent the actual measurements. It is important to mention here that the relative errors of the thrust, specific impulse and efficiency, which were deduced in chapter 3, are respectively:, $1.2\% \le \frac{\Delta T}{T} \le 2.3\%$, $2.3\% \le \frac{\Delta Isp}{Isp} \le 3\%$, $3.1\% \le \frac{\Delta \eta_T}{\eta_T} \le 5\%$. In order to obtain a clearer presentation of the results, the error bars were not drawn in the graphs.

Discharge Current

As can be seen from Figure 5.4, the discharge current is almost independent of the voltage in the 250-330 Volts range. This type of behavior, which is typical for Hall thrusters [17, 19, 20, 32] is a result of the fact that when the axial electron current is minimal, the discharge current is determined mainly by the ion current, which in turns is determined by the mass flow rate. As can be seen, the increase in the discharge current is proportional to the increase in the mass flow rate. For example, at a discharge voltage of 300V, the ratio of measured discharge currents at mass flow rates of 0.96mg/s and 1.32mg/s (0.96/1.32=0.72) is 0.70. Hence, it follows apparently, that the increase of the mass flow rate for a given discharge voltage increases both the ion and electron currents. This behavior is typical for Hall thrusters [17]. As can be seen, there is almost no increase in the discharge current with the voltage from 250V to 330V, indicating that in this range the voltage almost does not affect the ionization.

Thrust, specific impulse and efficiency

Figures 5.4-5.5 demonstrates the increase in the thrust and Isp with the voltage due to the increased kinetic energy acquired by the accelerated ions. At each voltage, the thrust, Isp and efficiency increase with the mass flow rate. The increased efficiency with the voltage, demonstrated in Figure 5.5, indicates larger values of the voltage utilization, and hence higher voltage drop in the acceleration region. As can be seen from Figure 5.5, the specific impulse follows roughly the $\sqrt{V_d}$ dependence. For example, at a mass flow rate of 1.19mg/s (275W), the ratio of measured specific impulse at discharge voltages of 250V and 300V ($\sqrt{250/300} = 0.91$) is 0.88. At each voltage, the thrust, Isp and efficiency increase with the mass flow rate, as can be seen in Figures. 5.4-5.6. While for the thrust this dependence is obvious, the lower values of the specific impulse and efficiency at low mass flow rates are less expected at first sight. This behavior can be explained, at least partially as follows. As the mass flow rate is decreased, so does the axial electron current. Then the probability of ionization of the neutrals becomes lower and, as a result, also the propellant utilization. Thus, for example, at a mass flow rate of 0.95mg/s (V_d=300V, P_e=264W) a thrust of 12.2mN was measured, corresponding to a specific impulse of 1303sec and an efficiency of 29.6%. When the mass flow rate was increased to 1.43mg/s, the input power was 459 Watts and we obtained: T=23.1mN, Isp=1643sec and η=40.7%. The highest performance was measured at V_d=330V and $\dot{m}$=1.52mg/s. The measured thrust was 25.1mN, while the Isp and efficiency were respectively 1680sec and 42.1%.

Figures 5.7-5.22 demonstrate the discharge current, thrust, specific impulse and efficiency for channel lengths of 37, 40, 45, 52mm. In general, a typical behavior of the thruster was observed in the five channel length cases, as for the dependence of the performance on the voltage and the mass flow rate. The above results, for the 33mm channel length, holds for the other channel configurations. However, as can be seen from Figures 5.9-5.11 for the 37mm channel length, decreased efficiency was obtained while increasing the discharge voltage from 300V to 330V. This effect, and why it is different than the other channel length cases, is not understood at the moment.

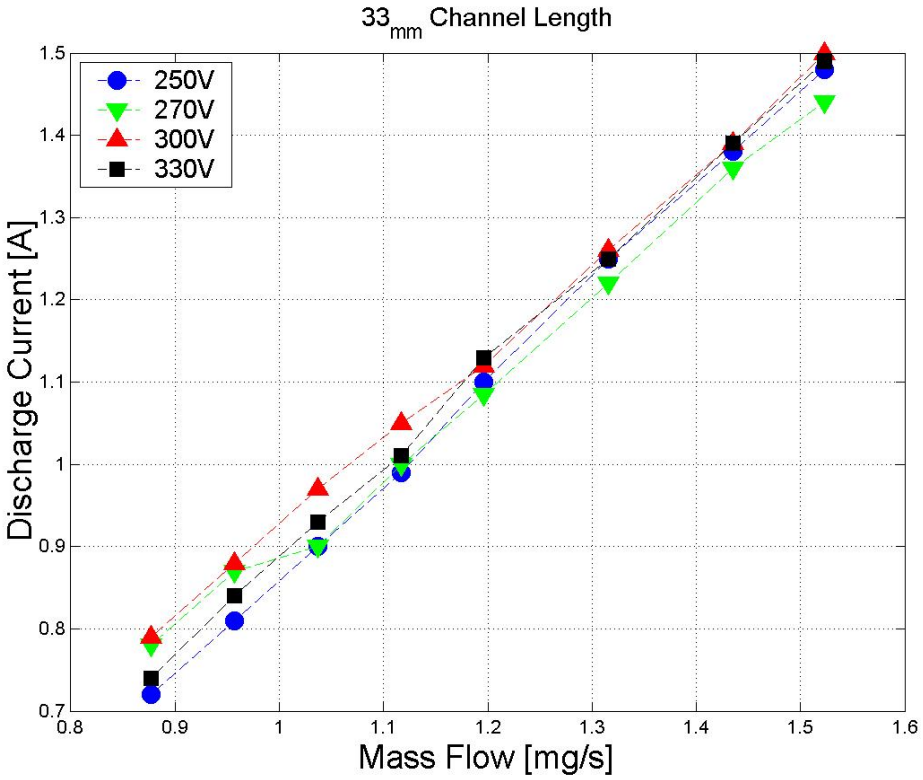

Figure 5.4: Measured discharge currents as functions of the mass flow at discharge voltage range of 250-330 Volts. The channel length is 33mm.

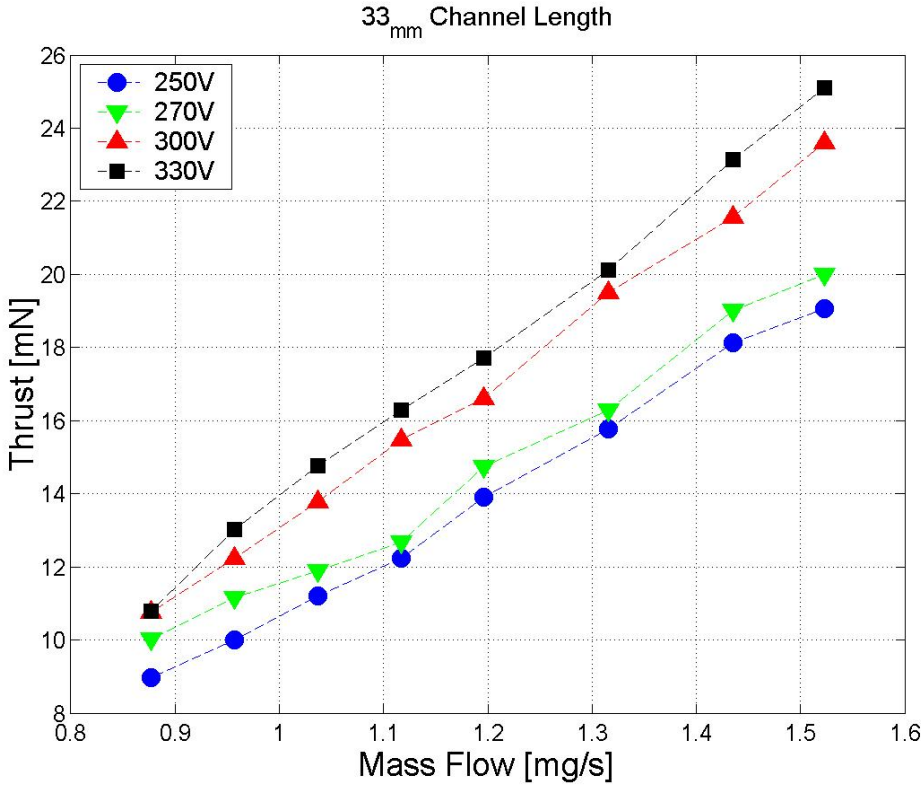

Figure 5.5: Measured thrust as a function of the mass flow rate at discharge voltage range of 250-330 Volts. The channel length is 33mm.

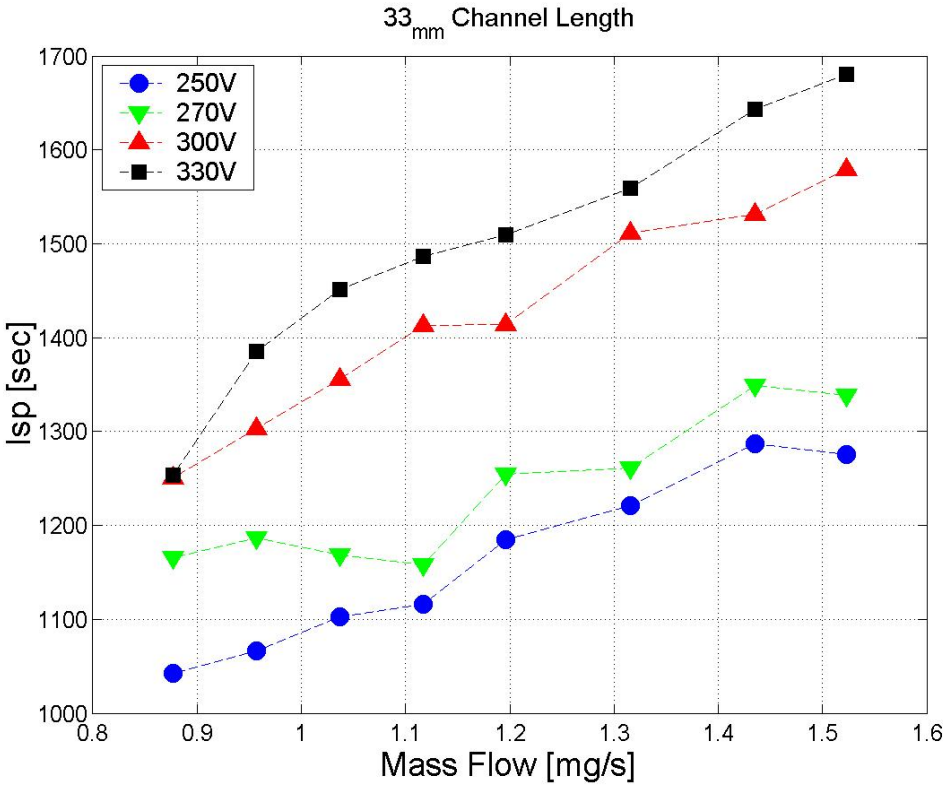

Figure 5.6: Specific impulse as a function of the mass flow rate at discharge voltage range of 250-330 Volts. The channel length is 33mm.

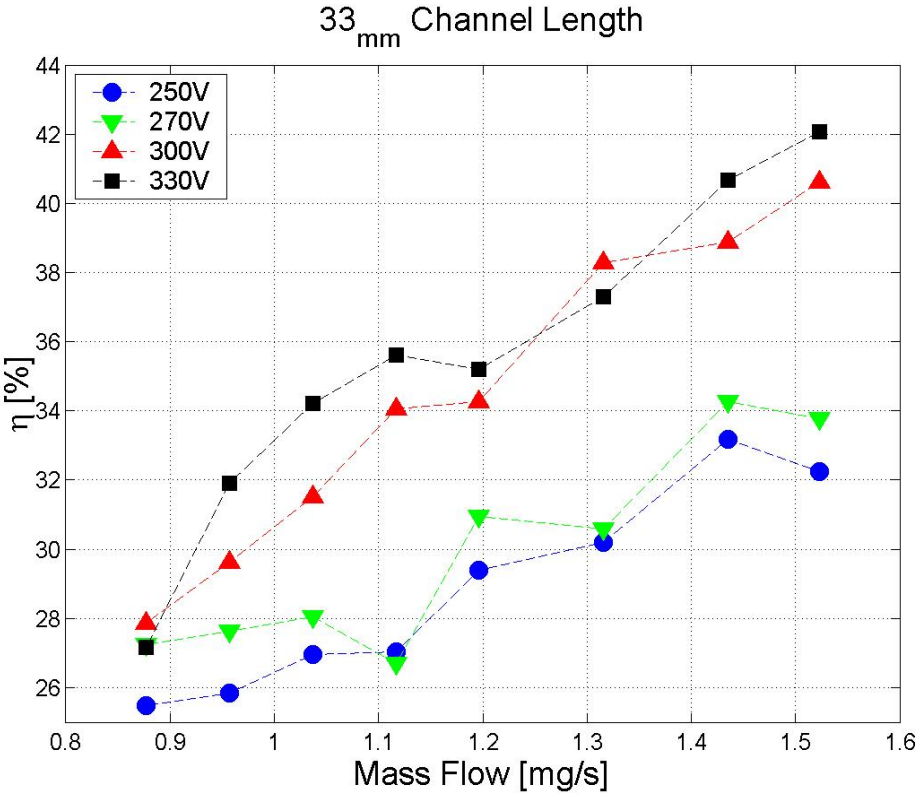

Figure 5.7: The thruster efficiency as a function of the mass flow rate at discharge voltage range of 250-330 Volts. The channel length is 33mm.

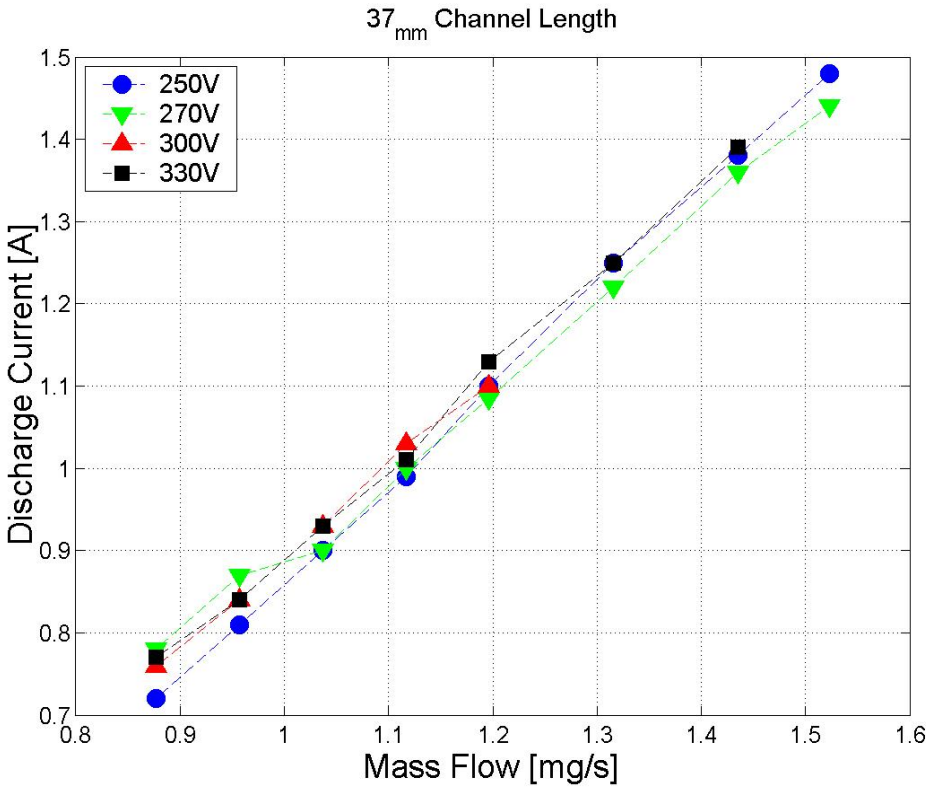

Figure 5.8: Measured discharge currents as functions of the mass flow at discharge voltage range of 250-330 Volts. The channel length is 37mm.

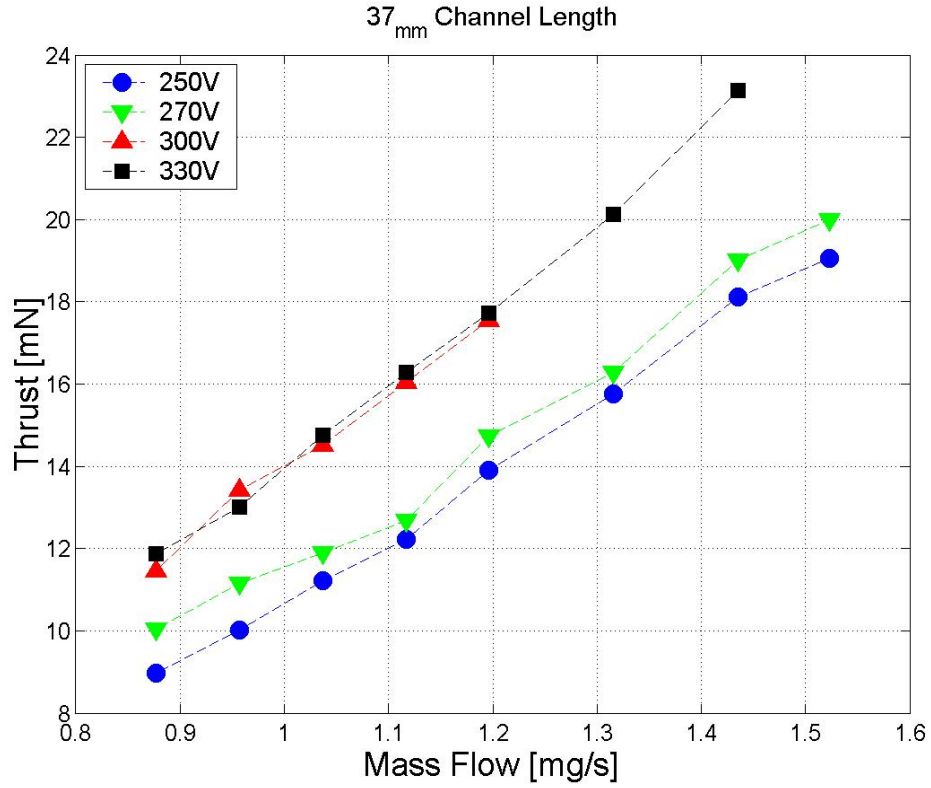

Figure 5.9: Measured thrust as a function of the mass flow rate at discharge voltage range of 250-330 Volts. The channel length is 37mm.

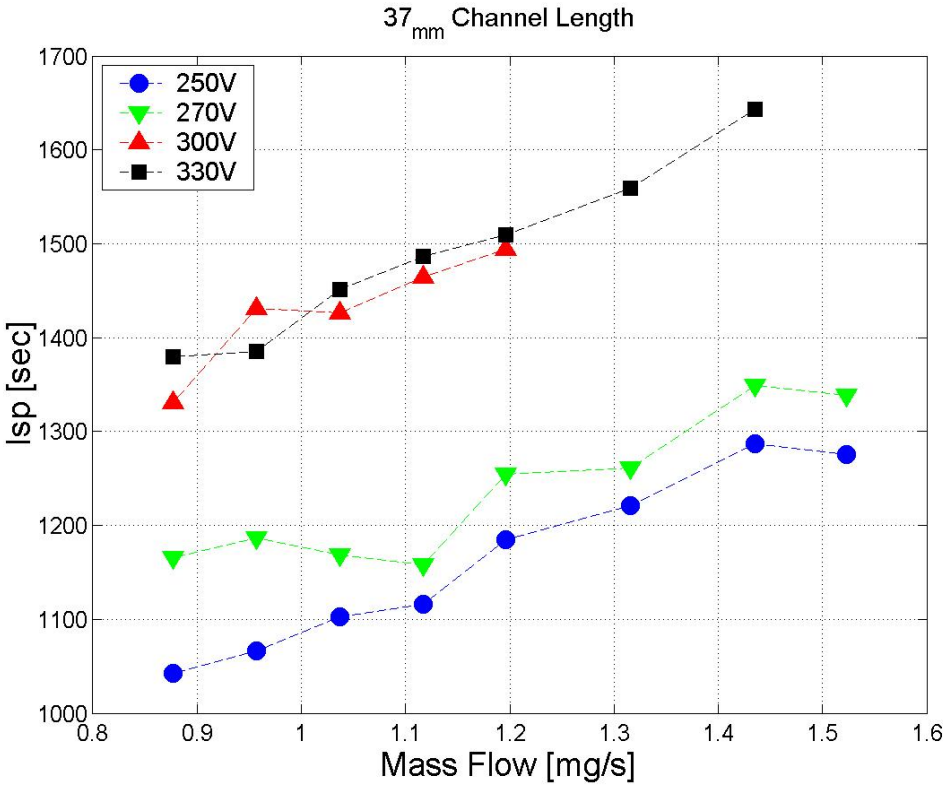

Figure 5.10: Specific impulse as a function of the mass flow rate at discharge voltage range of 250-330 Volts. The channel length is 37mm.

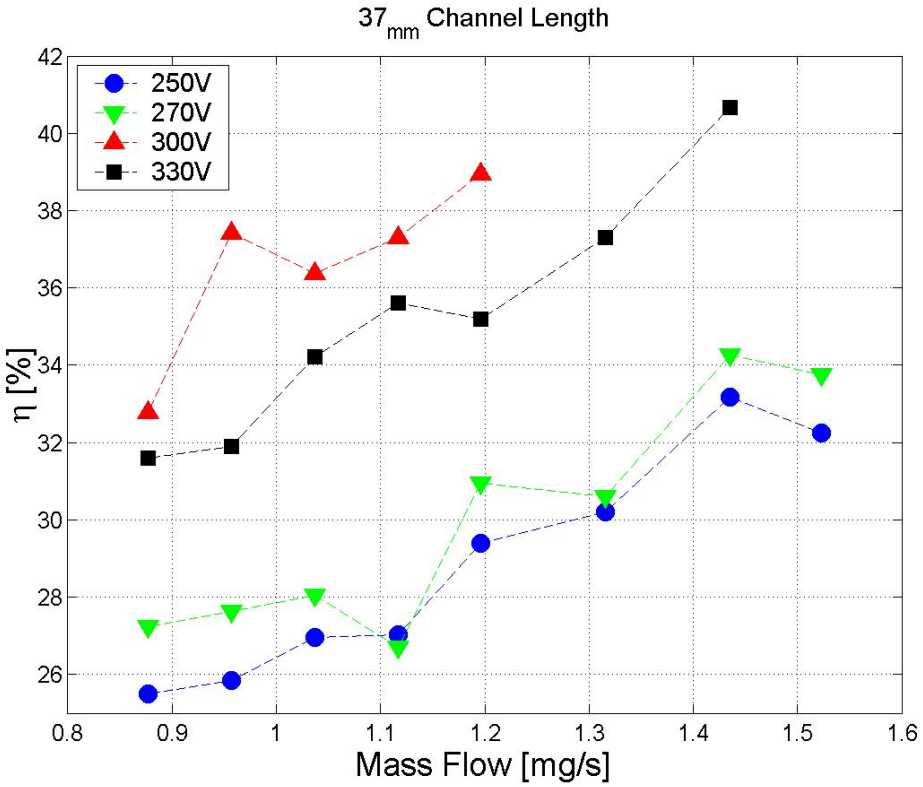

Figure 5.11: Thruster efficiency as a function of the mass flow rate at discharge voltage range of 250-330 Volts. The channel length is 37mm.

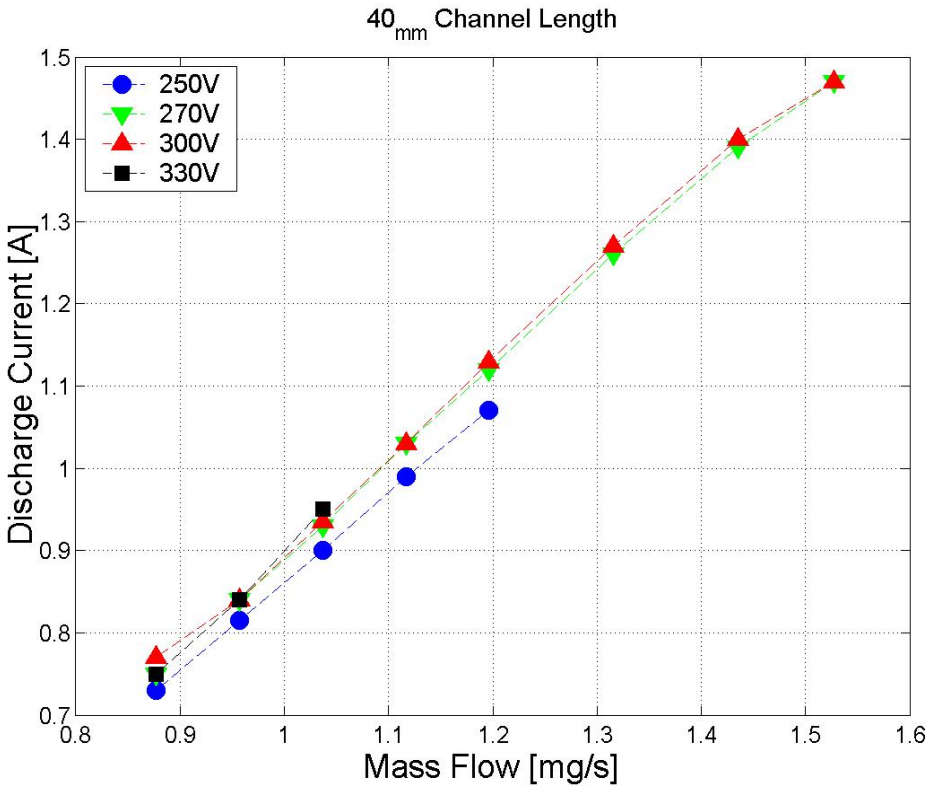

Figure 5.12: Measured discharge currents as functions of the mass flow at discharge voltage range of 250-330 Volts. The channel length is 40mm.

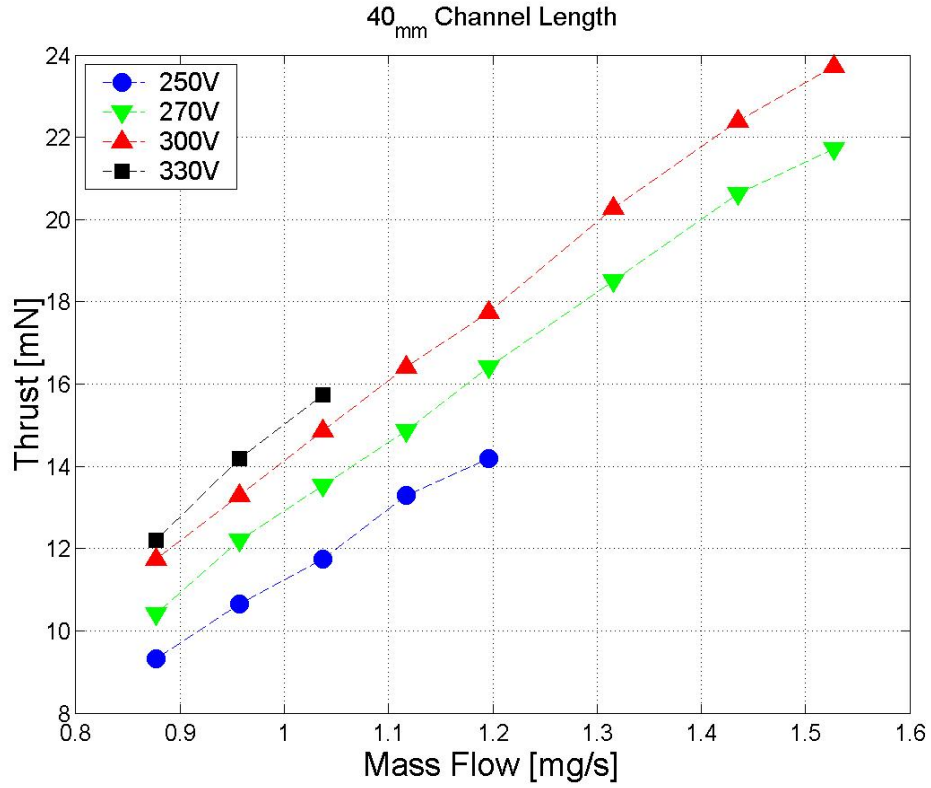

Figure 5.13: Measured thrust as a function of the mass flow rate at discharge voltage range of 250-330 Volts. The channel length is 40mm.

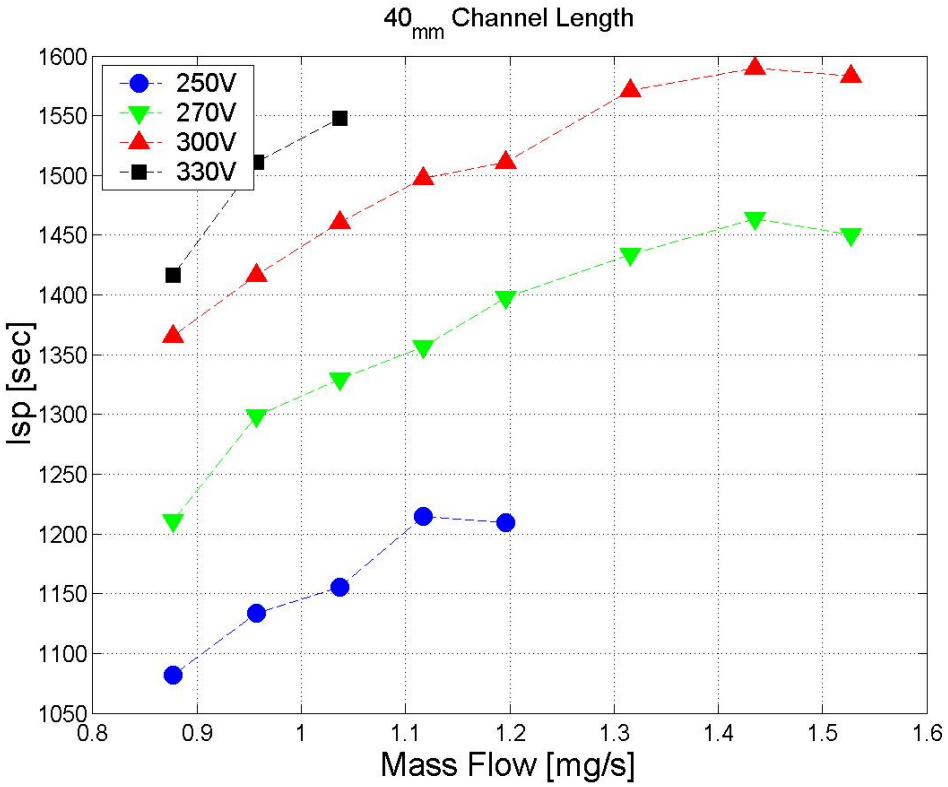

Figure 5.14: Specific impulse as a function of the mass flow rate at discharge voltage range of 250-330 Volts, in 40mm channel length.

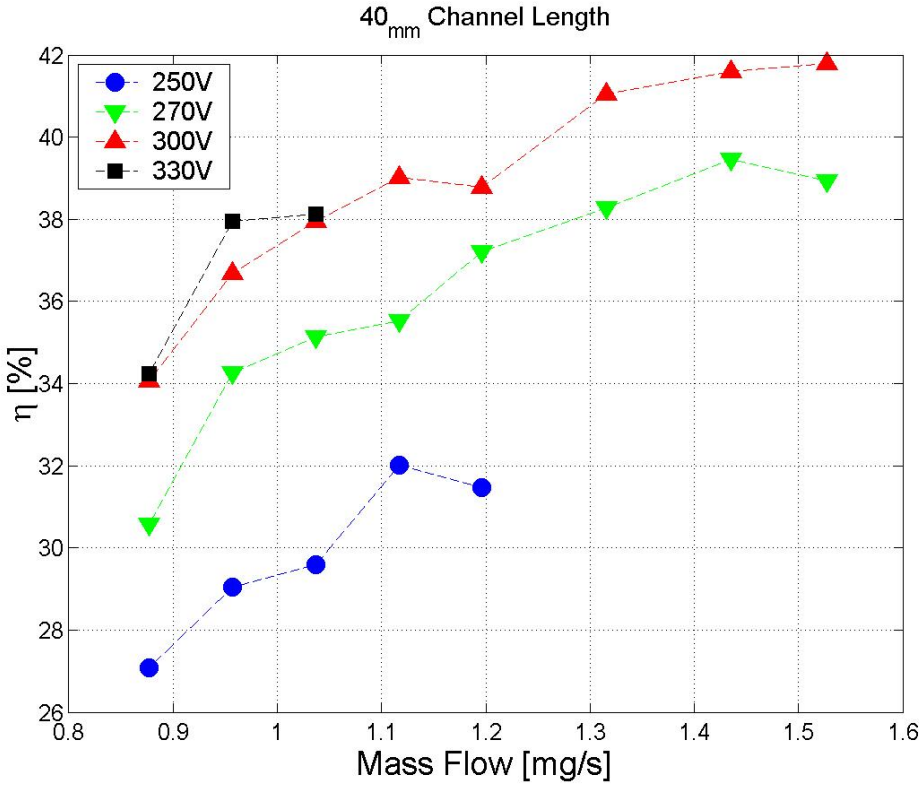

Figure 5.15: Thruster efficiency as a function of the mass flow rate at discharge voltage range of 250-330 Volts. The channel length is 40mm.

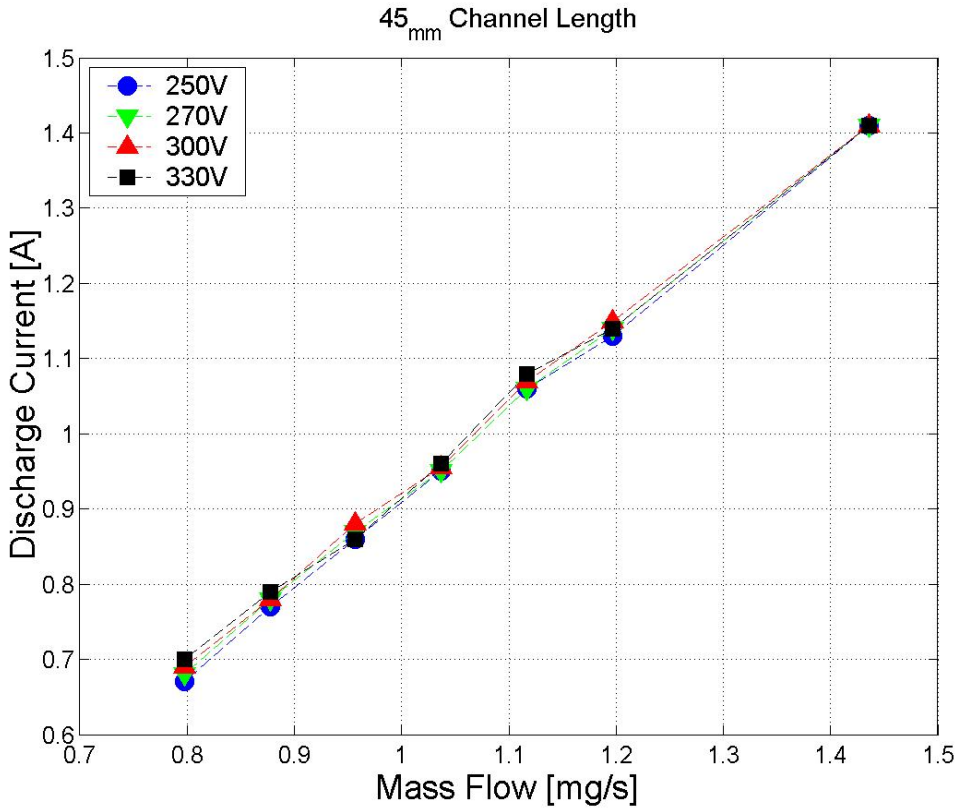

Figure 5.16: Measured discharge currents as functions of the mass flow at discharge voltage range of 250-330 Volts, 45mm channel length.

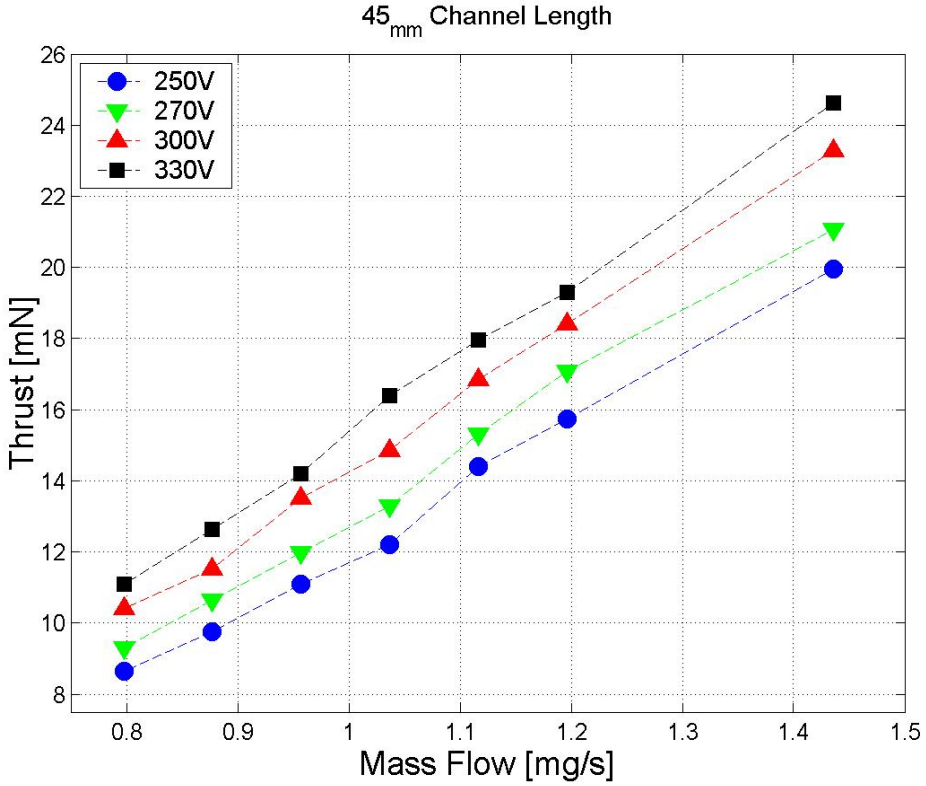

Figure 5.17: Measured thrust as a function of the mass flow rate at discharge voltage range of 250-330 Volts. The channel length is 45mm

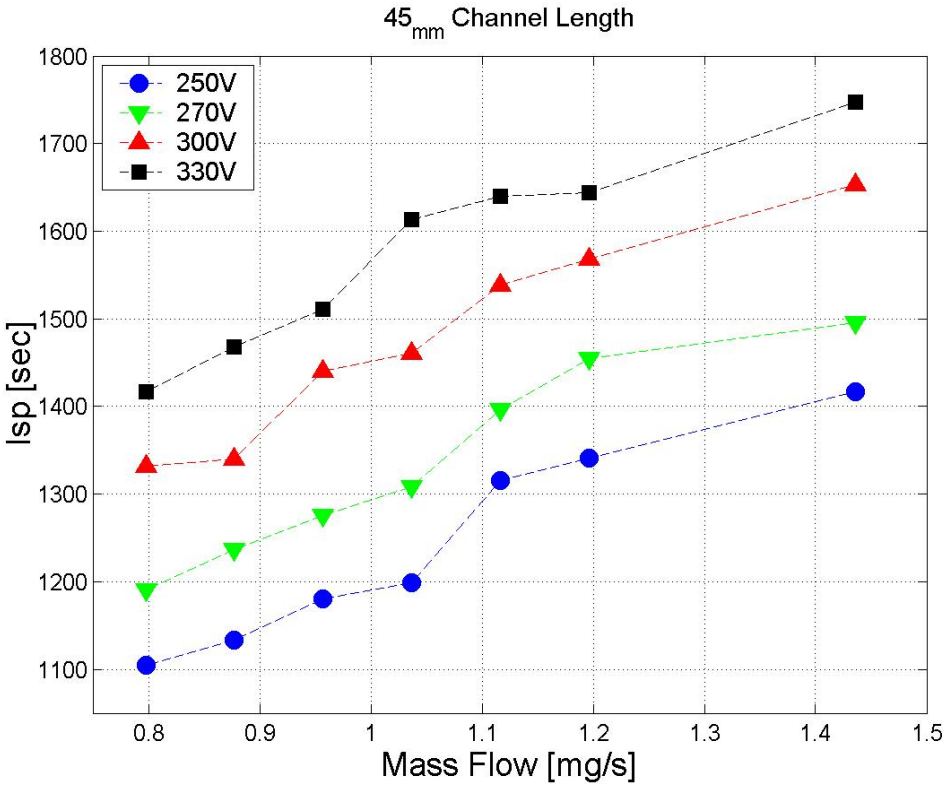

Figure 5.18: Specific impulse as a function of the mass flow rate at discharge voltage range of 250-330 Volts, in 45mm channel length.

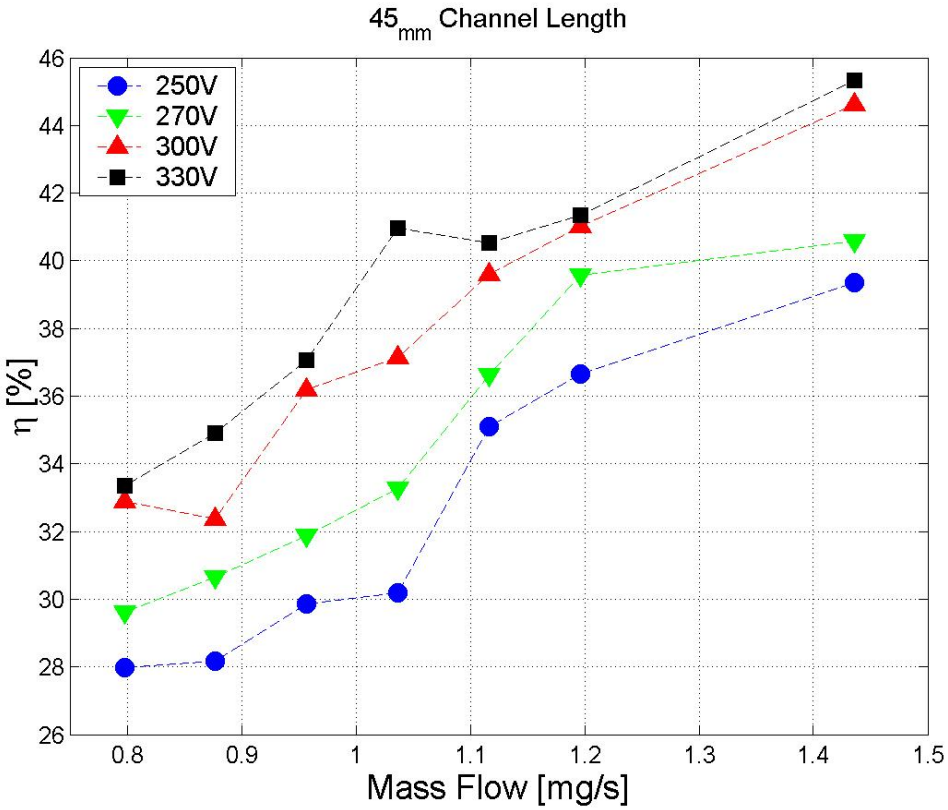

Figure 5.19: Thruster efficiency as a function of the **mass flow rate** at discharge voltage range of 250-330 Volts. The channel length is 45mm

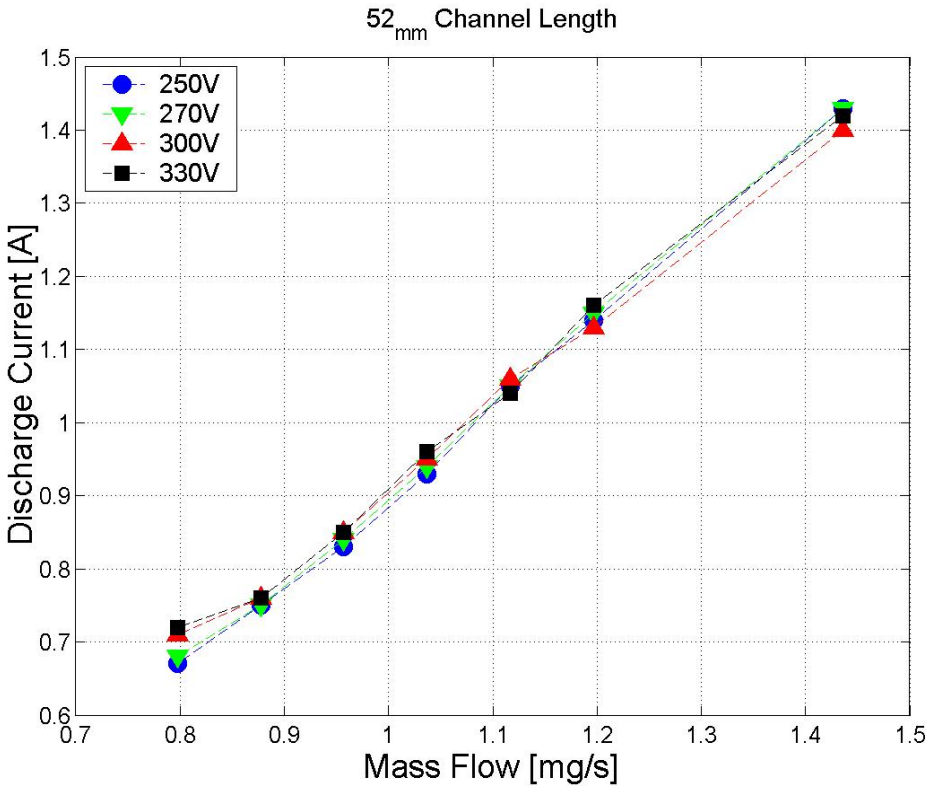

Figure 5.20: Measured discharge currents as functions of the mass flow at discharge voltage range of 250-330 Volts, 52mm channel length.

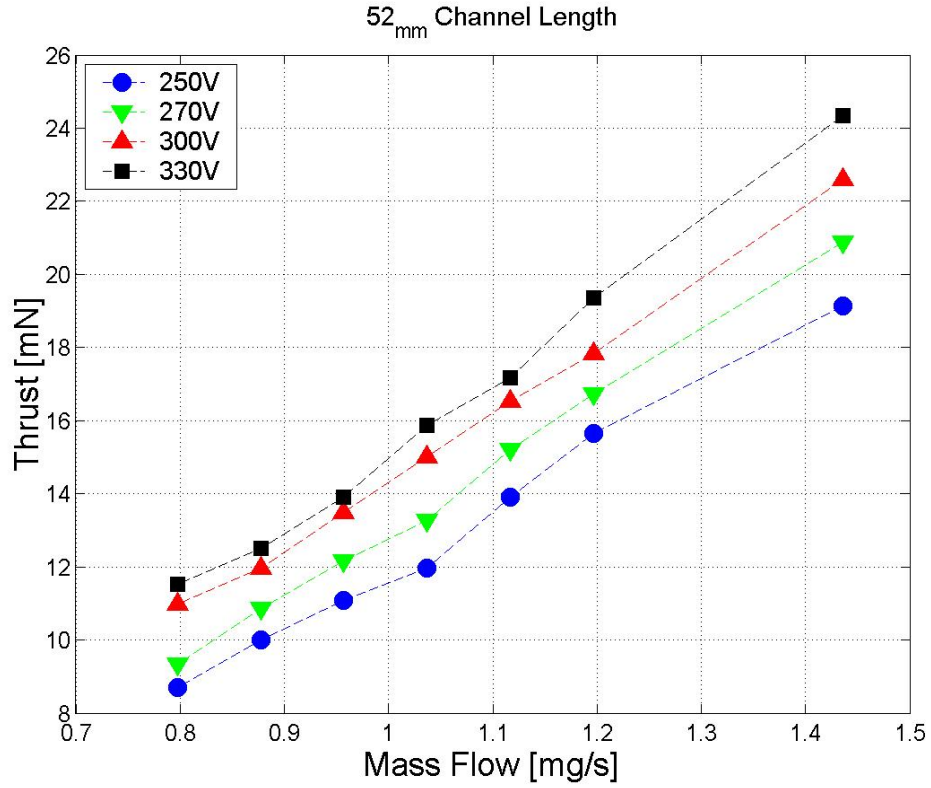

Figure 5.21: Measured thrust as a function of the mass flow rate at discharge voltage range of 250-330 Volts. The channel length is 52mm

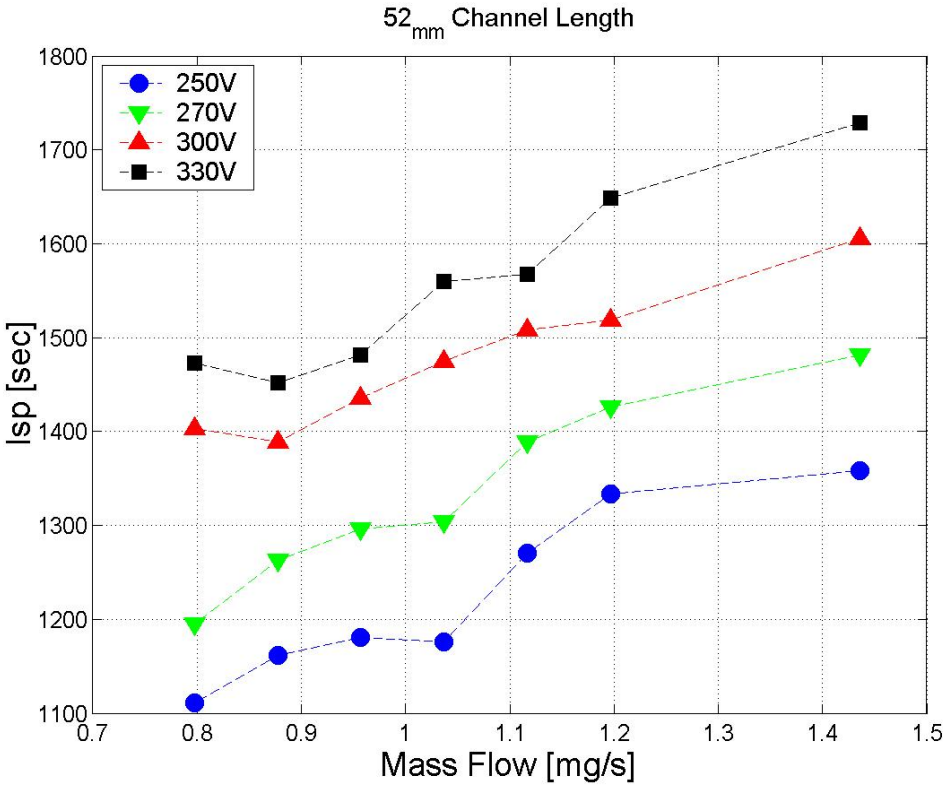

Figure 5.22: Specific impulse as a function of the mass flow rate at discharge voltage range of 250-330 Volts, in 52mm channel length.

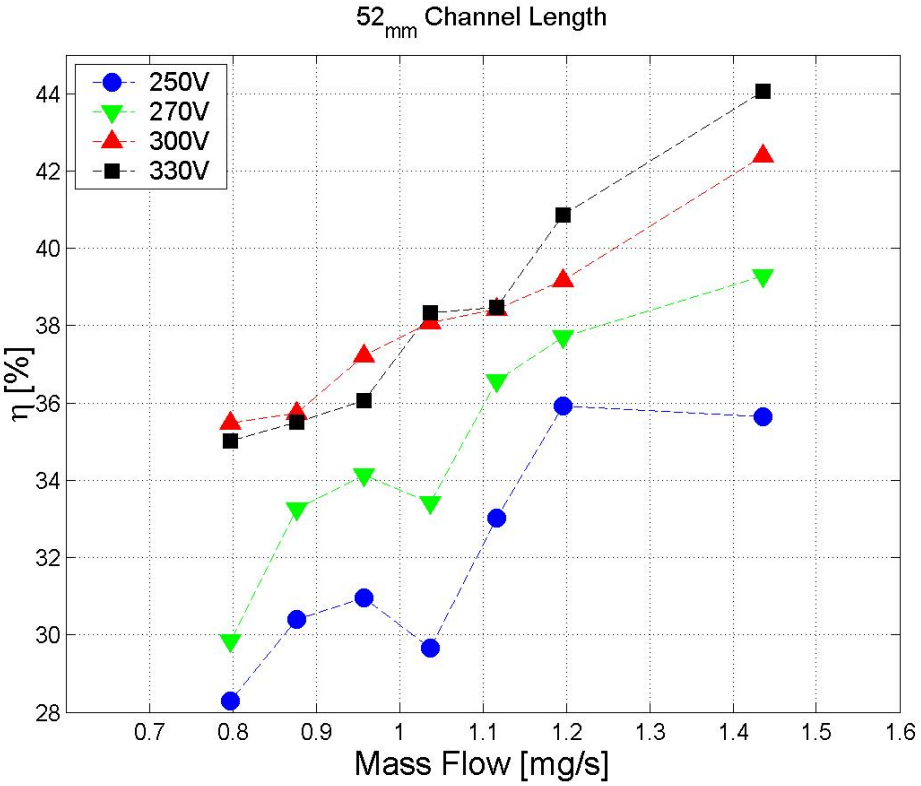

Figure 5.23: Thruster efficiency as a function of the mass flow rate at discharge voltage range of 250-330 Volts. The channel length is 52mm.

5.6 Comparison between Different Length Configurations and Discussion

In order to demonstrate the dependence of the thruster performance on the channel length, the discharge current, thrust, specific impulse and efficiency at 300V of the five channel lengths cases, are compared in Figures 5.24-5.28. As can be seen, an improvement in the thruster performance was observed when the channel was extended from 33mm to 40mm. For example, at L=33mm and an input power of 291 Watts (V_d=300V, $\dot{m}$=1.04mg/s) a thrust of 13.9mN was measured, corresponding to a specific impulse of 1370sec and efficiency of 32.2%, while at L=40mm and input power of 279 Watts (same operating condition, V_d and $\dot{m}$) a thrust of 14.9mN was measured, corresponding to a specific impulse of 1460sec and efficiency of 38.1%.

This improvement indicates that, most probably, the propellant utilization is increased in the extended channel. This improvement can be explained as follows. From Eq. (2.3) we can see that the characteristic ionization length is inversely proportional to the mass flow rate. Then, for a given channel length the ionization probability and, as a result, the propellant utilization are expected to increase with the mass flow rate. The relatively long characteristic ionization length at a low mass flow rate can be partially compensated by extending the channel length. An atom entering the channel through the anode has now a longer distance to travel until the channel exit, or being ionized by an impact of an electron.

When the channel was further extended to 45mm and 52mm only minor performance differences were observed. The almost similar performance results of the 40, 45 and 52mm channel length in the power range of 250-400 Watts indicate that for a specified mass flow rate there is a kind of "saturation" in the propellant utilization which can not be improved significantly by extending the chamber length more than 40mm. This behavior is different than the results described in [17] for the 400-700 Watts power range, from which it was suggested there that there is an optimal channel length, for a given mass flow rate. A possible explanation described in [17] for the existence of the optimal length was that recombination losses at the channel walls which act as a large "third" body compensate the improved ionization in the longer channel. The fact that in the 40-52mm channel lengths similar performance values were obtained seems to indicate that at even

lower mass flow rates there could be no advantage to go to even larger lengths. A possible additional loss mechanism that could explain this behavior is that the electrons, which have to travel a longer path towards the anode due to the elongated channel, have much less energy and thus are unable to ionize the Xenon atoms.

Finally, I would like to mention that, with no contradiction to the above, in the input power range of 200-250 Watts and discharge voltages of 300V, when the channel was extended from 33mm to 40mm and then to 52mm, some improvements were nevertheless observed in the specific impulse and efficiency as can be seen from Figures 5.24-5.26. For example, at a channel length of 33mm, at an input power of 215 Watts, (V_d=300V, $\dot{m}$=0.79mg/s) a thrust of 9.2mN was measured corresponding to specific impulse of 1180sec and efficiency of 25.5%. At the same discharge voltage and mass flow rate, at channel length of 40mm a thrust of 10.5mN was obtained corresponding to specific impulse of 1332sec and efficiency of 33.2%. In the case of the channel length of 52mm we obtained: T=11mN, Isp=1403sec, η=35.5%. This operating power is the lowest for which results are presented in this research work.

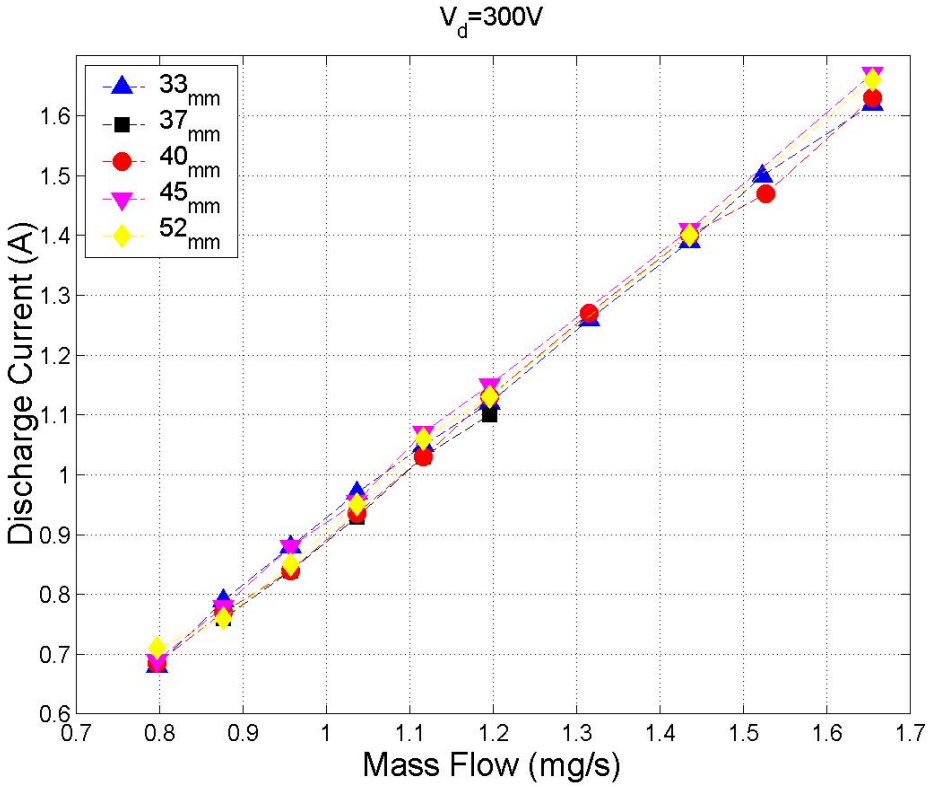

Figure 5.24: Measured discharge current, at a fixed discharge voltage of 300V, as a function of the mass flow rate for channel length range of 33-52mm.

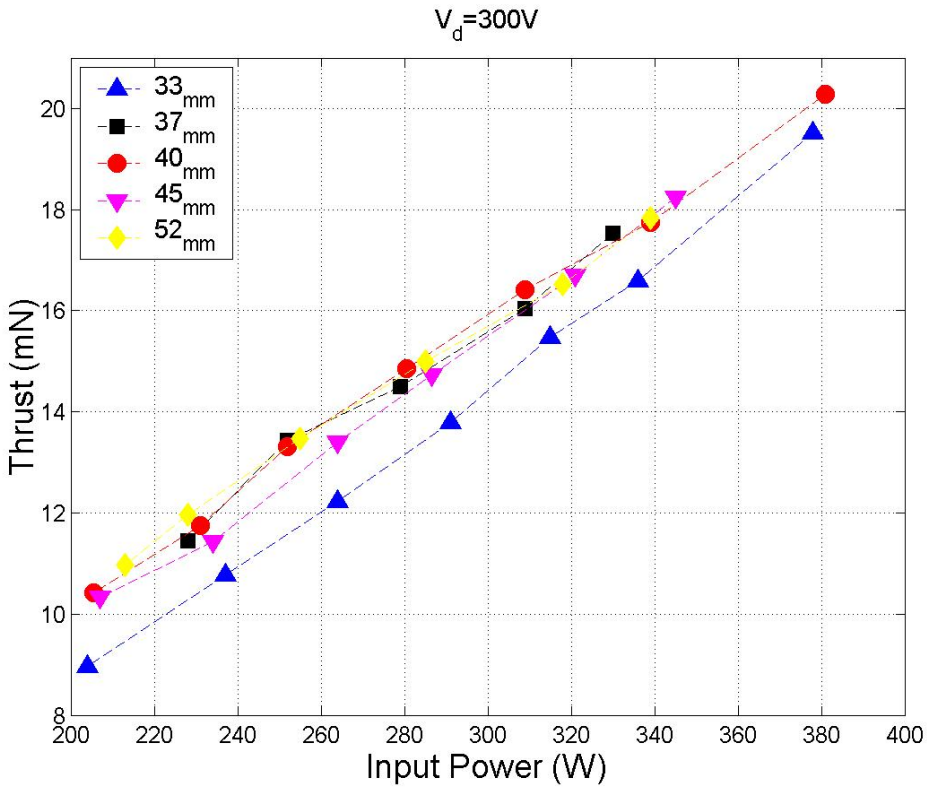

Figure 5.25: Measured thrust, at a fixed discharge voltage of 300V, as a function of the mass flow rate for channel length range of 33-52mm.

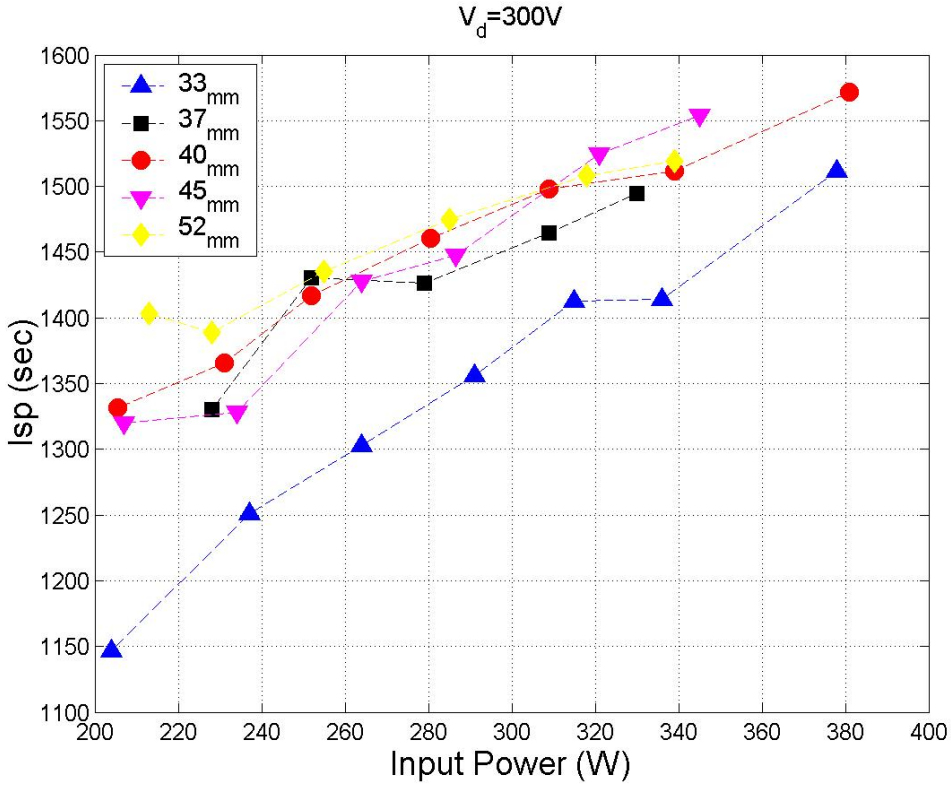

Figure 5.26: Specific impulse versus the electric input power for channel lengths of 33-52mm, at a fixed discharge voltage of 300V.

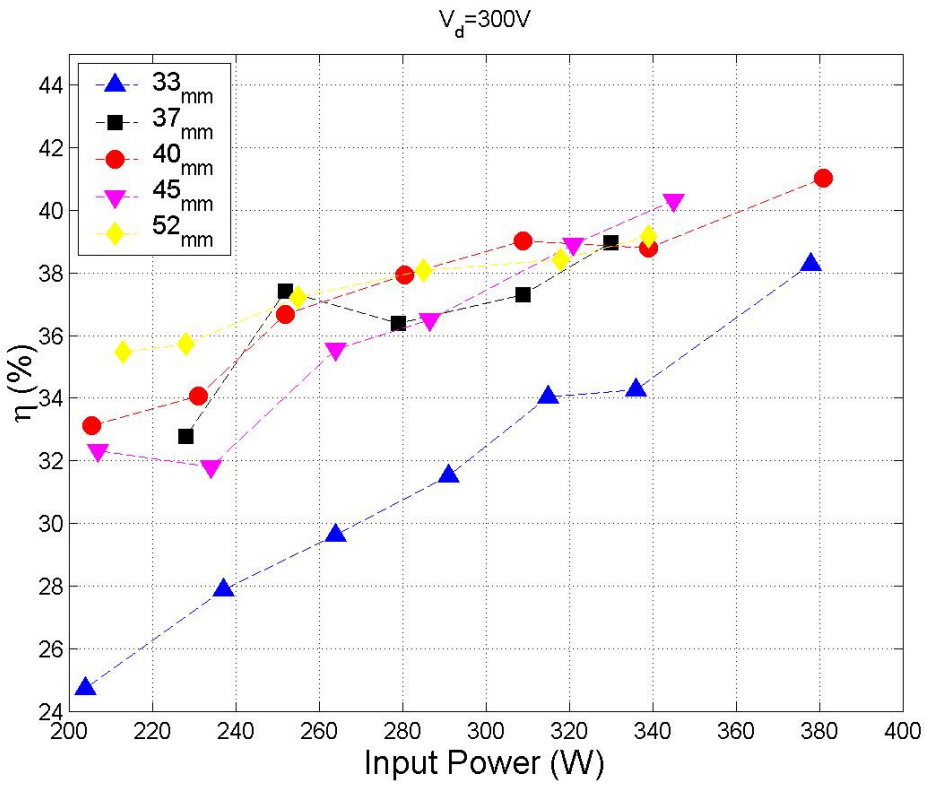

Figure 5.27: Thruster efficiency impulse versus the electric input power for channel lengths of 33-52mm, at a fixed discharge voltage of 300V.

5.7 Channel Length Variation - Summery

The improvement potential of Hall thruster performance at reduced power levels, by extending the length of the ceramic channel, was investigated experimentally with the improved laboratory Hall thruster. This investigation was motivated by the analysis in chapter 2 which showed that at reduced propellant flow rates, the efficiency of the ionization process drops as the effective distance over which this process takes place tends to increase. In addition, it was also shown that the thruster life time tends to increase when the thruster is operated at reduced power levels while the main drawback of down sized Hall thrusters in the power range below 300 Watts is the sharp reduction in the operating lifetime. The channel length was modified by locating the anode at different positions in an elongated channel. The channel was extended from 33mm length up to a length of 52mm. The performance for each of the lengths was measured in the power range of 200-400 Watts. Performance improvements were observed when the length was extended from 33mm to 40mm. When the channel was further extended only minor performance differences were observed. This particular finding, which was in opposite to the expectations, caused apparently due to the diminishing contribution of the electron at

an elongated channel. This study have shown that the initial assumption that at lower power levels there could be an advantage to go to even larger lengths, is limited While these results demonstrate that indeed the performance of the Hall thruster at reduced power levels can be improved by optimizing the channel length, the obtained improvements fall shorts of the performance of state-of-the-art larger power Hall thrusters.

Chapter 6

Reversed Magnetic Field Configuration

6.1 Design Objectives and Approach

As already mentioned in chapter 2, a problem associated with Hall thruster operation at reduced power levels is the degradation of thruster performance. When the operating power of a given Hall thruster configuration is reduced by lowering the discharge current its performance, namely the specific impulse and the efficiency, tends to degrade. This behavior is a result of the fact that lowering the current requires reducing the propellant flow rate thus leading to a lower propellant utilization. Due to the problems and difficulties associated with the scale down approach, a different approach was adopted in the research described in this work for Hall thrusters in the 200–300 Watts power range of trying to improve the propellant utilization of a 600 Watts thruster by modification of its configuration but without scaling it down. The improvement potential of Hall thruster performance at reduced power levels, by extending the length of the channel, was investigated experimentally. As described in chapter 5 applying this approach demonstrated improvements in the thruster performance, however these improvements fall shorts of the performance of state-of-the-art larger power Hall thrusters.

A second approach that was examined is to apply a higher magnetic field near the anode in order to decrease the axial electron velocity towards the anode and by that to increase their density and hence the probability of the neutrals to be ionized. However, an earlier attempt to broaden the magnetic field profile by increasing the magnetic field near the anode resulted in a reduced efficiency [27]. Most probably, the ion losses increased with the length of the acceleration region. To overcome this problem, Prof. Amnon Fruchtmann, who collaborates with Soreq on the theory of Hall thrusters, have suggested a novel idea, to apply near the anode a magnetic field with an opposite sign to that of the field near the exit. Such a magnetic field profile has a higher gradient towards the exit, which could probably result in a better focusing of the plume, and hopefully will lead to

higher thruster efficiencies. The objective of the research work described in this chapter was to modify the magnetic circuit in order to attain a reversed magnetic field near the anode, to test this configuration in order to validate that it operates as a thruster and to perform preliminary characterization of the thruster performance.

6.2 Implementation of the Reversed Magnetic Field Configuration

In this work, a reversed magnetic field distribution was attained by modifying the rear part of the magnetic circuit to allow a penetration of magnetic field lines directed opposite to the field lines near the anode, and thus creating a sharp gradient of the magnetic field in the acceleration region. This implementation of this magnetic field is a relatively simple solution which allows to operate the thruster with a constant magnetic profile for preliminary measurements.

In order to study and optimize the new magnetic circuit design, a 2-D axisymmetric model of the magnetic circuit was designed. A finite-element software package was used to model the magnetic circuit, simulate the field distribution and learn how to create the desired magnetic field by using the laboratory model Hall thruster with minimum changes to the magnetic circuit parts. The magnetic field distribution was mapped with a digital Gauss-meter using a two axis Hall probe. Measurements performed in many cuts in the *r, z* plane demonstrated a very good agreement with the simulated radial field distribution. Figure 6.1 shows the simulated and measured radial magnetic field distributions at the channel median. In this graph, the origin is at the back plate of the magnetic circuit. As can be seen there is a very good agreement between the measured and the simulated B_r profiles. The azimuthal homogeneity of the field distribution was also checked. Between the poles, a variation of ±1% was observed for both B_r and B_z. In order to investigate the magnetic field strength inside the iron parts, especially the four external core rods, a 3-D simulation was also made, using the software COSMOSEMS.

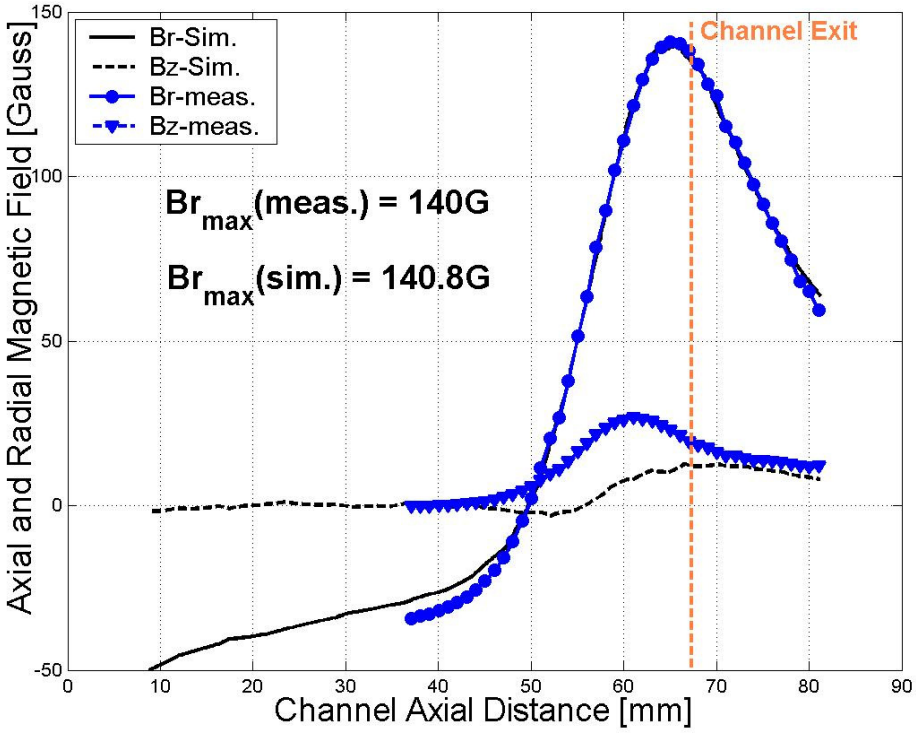

Figure 6.1: Measured and simulated results of the axial and radial magnetic field distribution at the channel median. The results were taken with Ic=2.5A.

As can be seen in Figure 6.1, the radial magnetic field reaches the maximum value near the channel exit and drops rapidly while changing its direction 15mm from the channel exit towards the anode. From this point to the anode, the magnetic field is increased until it reaches a value of about -35 Gauss near the anode. One can see that this magnetic field distribution is different than the standard magnetic field profile presented in Figure 4.7. For similar coils current to that applied with the standard magnetic circuit a reduction of ~25% in the magnetic field strength was observed. For example, the measured maximal magnetic field in the standard configuration was 140 Gauss compared to 115 Gauss with the gap at a coils current of 2A. In order to achieve the same maximal magnetic field value, an increased coils current was needed. According to simulations the increased coils current results in a 25% higher magnetic flux in the iron parts, although it does not approach the saturation value (~15KG).

6.3 Preliminary Measurements

This section describes a preliminary set of measurements with the reversed magnetic field profile. Three thruster length configurations were checked, 33, 40 and 52mm at a discharge voltage of 300 Volt and mass flow rate range of 0.8-2 mg/s. Under these conditions electrical properties and thrust were measured from which the thruster discharge characteristics, specific impulse and efficiency were deduced. The performances which are presented were taken without including the cathode mass flow rate. All the measurements were taken with a clean anode. A summery of the preliminary thruster performance results appears in Figures 6.2-6.4. In general, most of the measurements were performed with the 33mm channel length configuration, although the thruster was operated with the 40 and 52mm configurations at a few working points in order to verify that it works as a thruster.

Unlike the standard thruster, this thruster with the modified magnetic field was started immediately even without decreasing the coils current (to increase the axial electron current) and the thruster operation was stable at most of the operating conditions and input power levels checked. Two kinds of different modes were observed during the thruster operation. The first is characterized by a minimum discharge current, which usually corresponds to maximal specific impulse and efficiency, but it was associated with high oscillations where the peak to peak amplitude of these oscillations, for example at I_c=1.8A, is approximately 50% of the DC current. For comparison, the oscillations amplitude in the standard thruster was about 10% of the DC current. As the coils current is increased, which results in an increased magnetic field, the oscillations were reduced but the discharge current is significantly increased by about 200mA more than the first mode. This behavior is not yet understood. A majority of the measurements were performed at the operating point corresponding to the first mode described above. In most operating points, especially in the lower mass flow rate range, higher discharge current values, by 20-40mA compared with measured values in the standard 33mm configuration, were measured. When the mass flow rate was increased the discharge current values were almost the same as for the standard thruster. Since the efficiency of the thruster is dependent on the discharge current, the increased discharge current damaged the overall thruster efficiency, as is presented in Figure 6.4.

Interestingly, a much narrower erosion region was observed. The original color of the ceramic channel is white, while it turns black during thruster operation due to the deposition of carbon and steel particles. In the acceleration region, however where most of the voltage drop occurs, the erosion of the ceramic channel due to impact of energetic ions results also in the cleaning of the black deposited material. As a result, after many hours of operation the white eroded region is clearly visible. The modified magnetic field thruster operated with the same discharge chamber that was used before within the standard thruster with the length dependence parametric study and about 30% of the originally white area was coated. Most probably, this discovery indicates that the energetic ions impact a narrower region in the modified magnetic field configuration. This result could possibly be an outcome of the better focusing expected for this magnetic profile, however additional diagnostics of the ion jet are needed in order to verify this point.

Figure 6.2 demonstrates the increase in the thrust when the propellant flow rate is increased at a discharge voltage of 300V. The results of the reversed magnetic field are compared with the standard configuration measurements. Lower thrust levels (0.5-2mN) were measured in the power range of 200-600 Watt, compared to the standard thruster with 33mm channel length. Although the eroded area at the channel exit is narrowed, the thrust level is lower. A possible explanation is that, the electron density near the anode due to the increased magnetic field results in a voltage drop there, which supposedly may decrease the potential in the accelerating region. It could be then that there is an optimal magnetic field for which the thruster performances are maximized.

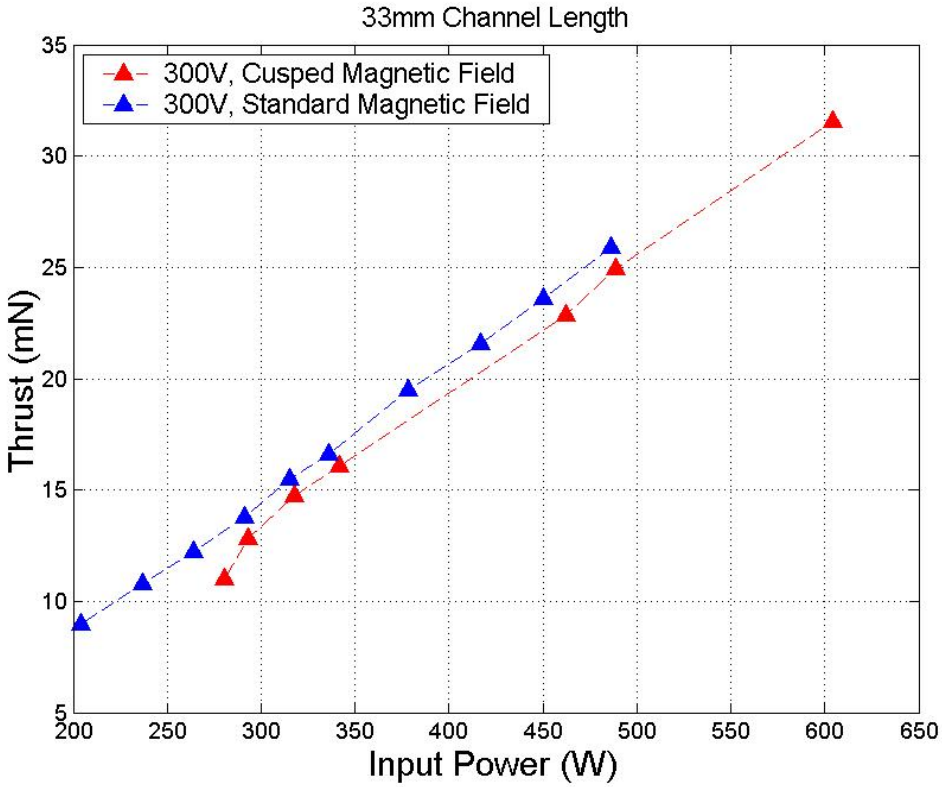

Figure 6.2: Measured thrust versus electric input power for discharge voltage of 300 Volt.

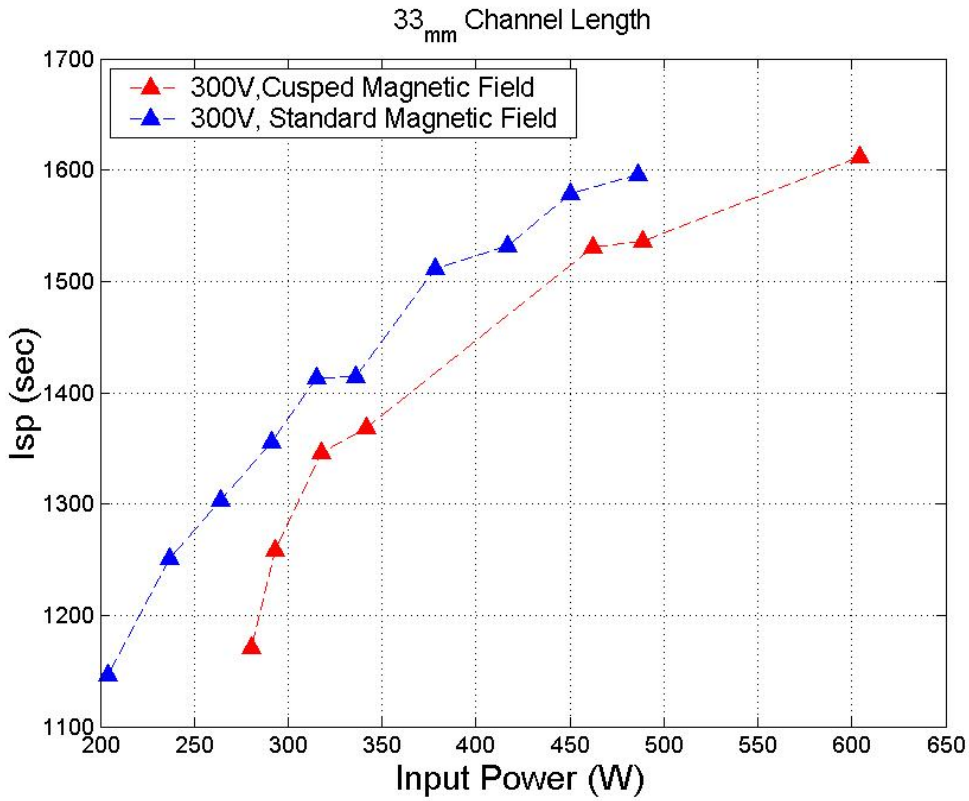

Figure 6.3: Specific impulse versus input power for discharge voltage of 300 Volt.

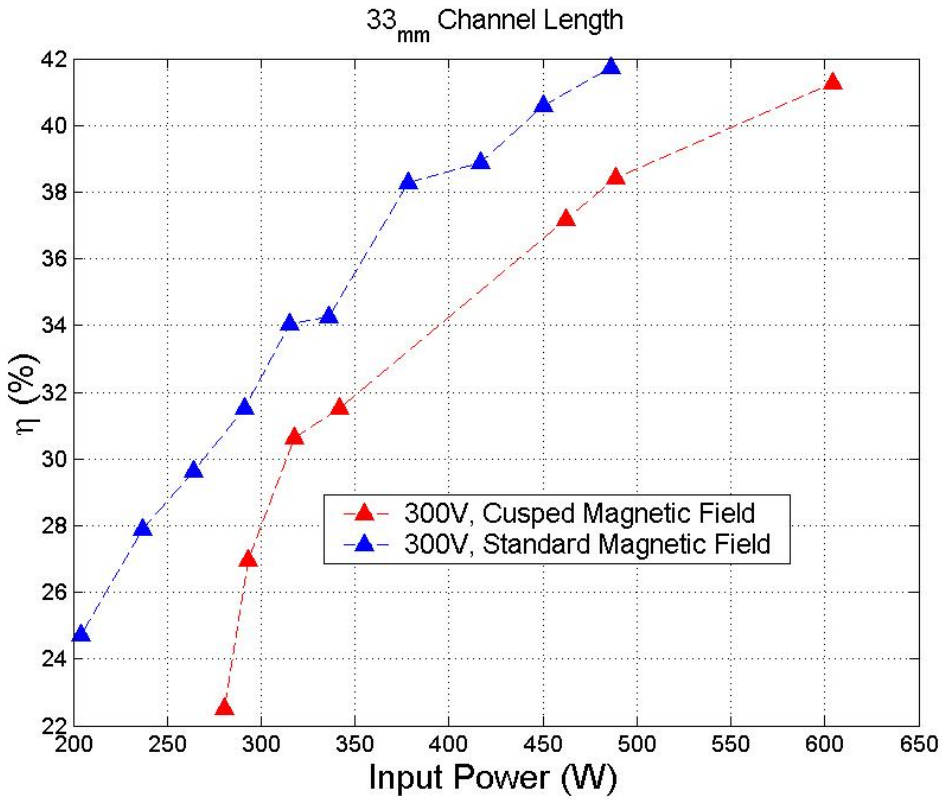

Figure 6.4: Efficiency versus electric input power for discharge voltage of 300 Volt.

Chapter 7

Conclusions

This work deals with the performance of low power (200-300W) Hall thrusters. The problem associated with Hall thruster operation at reduced power levels is the degradation of thruster performance. When the operating power of a given Hall thruster configuration is reduced by lowering the discharge current its performance, namely the specific impulse and the efficiency, tends to degrade. This behavior is a result of the fact that lowering the current requires reducing the propellant flow rate thus leading to a lower propellant utilization. The standard approach to restore the high propellant utilization when the power is reduced is to scale down the thruster size. Scaling of existing thrusters to allow operation at low power is not a novel approach. In most cases, scaling was implemented as "photographic" reduction in the thruster dimensions or "cross-sectional" scaling, or as a set of variations in the power level, magnetic field distribution, and the mass flow rate to achieve optimal performances. The present work presents a simplified analysis, of two of these scaling strategies under the requirement to preserve the overall thruster efficiency. As the analysis showed, the implementation of scaled down thrusters requires an increased magnetic field while the reduced thruster geometry is limited due to volume constraints of the magnetic circuit and saturation of its iron parts. It is also shown that the main drawback of down sized Hall thrusters in the power range below 300 Watts is the sharp drop in their operating lifetime compared to larger size thrusters.

Due to the problems and difficulties associated with the scale down approach, in this research work a different approach for Hall thrusters in the 200–350 Watts power range was adopted. This approach is to improve the propellant utilization of the 600 Watts thruster by modification of its configuration without scaling it down. This approach has the advantage of avoiding the short reduction in the operating lifetime, and maybe even extending it. A straightforward implementation is to extend the channel length of the thruster. According to the analysis in chapter 2, the channel length must be longer than

the characteristic ionization length in order to obtain good ionization efficiency. Therefore, extending the length of the channel can serve as an alternative to the geometrical scaling approach as a mean to overcome the propellant utilization problem when the mass flow rate is reduced. The implementation of this approach necessitated a design and construction of an improved laboratory Hall thruster which is appropriate to the extended channel experiments. The thruster performance for five channel lengths was measured at the 200-350 Watts power range for various voltages and propellant flow rates. Performance improvements were observed when the channel length was extended from the original (33mm) up to the 40mm. However, in an input power of ~300W, when the channel was further extended up to 52mm, the changes in the thruster performances were very small.

The thruster operation in a reduced mass flow rate results in decreased thrust which reduced the accuracy of the thrust measurement. Since the uncertainty in the thrust measurement is partially due to the limited calibration accuracy, an improvement in the calibration system was certainly needed. Prior to this work, calibration could be performed only when the vacuum chamber was open and the thrust stand accuracy was limited by the scatter in calibrations between consecutive chamber openings which was 2-3%. To improve the accuracy and, as well, to reduce uncertainties related to the conditions inside the vacuum chamber during cryopumps and thruster operation, a dynamic calibration system, which allows to calibrate the thrust stand during cryopumps and thruster operation, was designed and built. The dynamic calibration and accumulated experience allowed reducing the relative error in the thrust stand calibration from ~2.5% to less than 0.5%, corresponding to a reduction in the thrust relative error from 3.1% to ~1.9% (thrust of 12mN).

Finally, this work includes the design, and construction of a modified thruster, in which a reversed magnetic field is used in order to increase the electron density near the anode. Applying a negative magnetic field near the anode could keep a narrow acceleration region by a sharp gradient magnetic field. This modified magnetic circuit is based on the SLM-2 magnetic circuit, except for minor changes in the magnetic circuit in order to achieve the desired magnetic field distribution near the anode. The magnetic field distribution was mapped. Measurements performed in many cuts in a *r,z* plane demonstrated a very good agreement with the simulated field distribution. In this work, a

preliminary set of measurements is described. Lower thrust levels (0.5-2mN) were measured in the power range of 200-600 Watt, compared to the standard 33mm thruster. Higher discharge current were measured compared with those measured in the standard 33mm configuration, in most operating points, especially in the reduced mass flow rates. Since the efficiency of the thruster depends on the discharge current, the increased discharge current damaged the overall thruster efficiency. It is important to mention that a much narrower erosion region was observed, compared with the standard thruster configuration. Most probably, this discovery indicates that the energetic ions impact a narrower region in the modified magnetic field configuration. This result could possibly be an outcome of the better focusing expected for this magnetic profile.

The initial set of measurements of the reversed magnetic field configuration, have shown a great deal of promise. An improved reversed magnetic field configuration which allows varying the magnetic field near the anode without damaging the magnetic profile near the exit is under design. In addition, development of diagnostic probes to measure the ion flux and energy which allow characterizing the voltage, propellant and current utilizations independently, are needed in order to better understand the physics of the thruster. Meanwhile, alternatives to improve the thruster performance at reduced power levels are planned, including the variation of the profiles of the channel cross-section and anode modifications.

References

1. J. Ashkenazy, Y. Raitses and G. Appelbaum, "Electric Hall Thruster Reasearch & Development at Soreq", *Israel Annual Conference on Aerospace Sciences*, Feb. 1995.
2. M. Guelman, J. Ashkenazy and Y. Raitses, "From Earth to Moon with Electric Propulsion", *Israel Annual Conference on Aerospace Sciences*, October. 1994.
3. William Anthony Hargus, Jr., "Investigation of the plasma acceleration mechanism within a coaxial Hall thruster", Report No. TSD-130, March 2001.
4. J. R. Bettie and J. P. Penn, "Electric Propulsion as a National Capability", *Aerospace America*, pp. 56-59, July 1990,.
5. J. Ashkenazy, "Electrical Propulsion for Space Missions" (in Hebrew), Soreq NRC report Num. 2067, 1990.
6. D. G. Fearn, "Electric Propulsion of Spacecraft", Royal Aircraft Establishment Technical Report 81131, October 1981.
7. B. Arkhipov, A. Bober, M. Day, R. Gnizdor, K. Kozubsky, N. Maslennikov, "Extending the range of SPT operation-Development status of 300 and 4500 Watts thruster", AIAA-96-2708, 32nd *Joint Propulsion Conference*, Lake Buena Vista, FL, July 1-3, 1996.
8. D.H. Manzella, S. Oleson, J.Sankovic, T.Haag, A. Semenkin, and V. Kim., "Evaluation of Low Power Hall Thruster Propulsion", AIAA-96-2736, 32nd *Joint Propulsion Conference*, Lake Buena Vista, FL, July 1996.
9. http://www.search.nasa.gov
10. M. D. Rayman, "Results From The Deep Space 1 Technology Validation Mission", AIAA -99, California Institute of Technology, Pasadena, California, 91109
11. R. L. Poesched and J. Hyman, "A comparison of Electric Propulsion Technologies for Orbit Transfer, in Orbit-Raising and Maneuvering

Propulsion: Research Status and Needs", L. H. Caveny Ed., *Progress in Astronautics and Aeronautics*, Vol. 89, pp. 203-232 (1984).

12. G. D. Voulelikas, "Electric Propulsion: A Review of Future Space Propulsion Technology", Communications Research Center, Dept. of Communications, Canada, CRC Report No. 1396, October 1985.
13. http://www.amsat.org/amsat/sats/phase3d/atos.html.
14. J. Ashkenazy, Y. Raitses, and G. Appelbaum, "Investigations of a Laboratory Model Hall Thruster", AIAA-95-2673, *31st Joint propulsion Conf.,* San Diego, CA, July 1995.
15. F. F Chen, "Plasma Physics and Controlled Fusion",Vol. 1:Plamsa Physics, 2nd ed., Plenum Press, 1984.
16. Y. Raitses, J. Ashkenazy and M. Guelman, "Propellant Utilization in Hall Thrusters", AIAA *Journal of Propulsion & Power*. 14, 247, 1998.
17. Ashkenazy, J., Raitses, Y. and Appelbaum, "Parametric Studies of the Hall Current Plasma Thruster," *Physics of Plasmas,* Vol. 5, No. 5, 1998, pp. 2055-2063.
18. M.B. Belikov, O.A. Gorshkov, V.A.Muravlev, R.N. Rizkhanov, A.A. Shagayda, and A.U.Shnirev., "High-Performance Low Power Hall Thruster", AIAA-2001-3780, *34th Joint propulsion Conf.,* Salt Lake City, Utah, July 2001.
19. Y. Raitses, "Investigation of the Hall Thruster and Its Use for Satellite Drag Compensation", Research Thesis, June 1997.
20. V. Hruby, J. Monheiser, B. Pote, C. Freeman and W. Connolly, "Low Power, Hall Thruster Propulsion System", IEPC-99-092, Japan, October 1999.
21. Ashkenazy, J., Raitses, Y. and Appelbaum, G., "Low Power scaling of Hall Thrusters," *Proc. of 2nd European Spacecraft Prop. Conf. ,* Noordwijk, Holland, May 1997, pp.455-460.
22. E. Ahedo and J.M. Gallardo, "Scaling down Hall thruster", IEPC-03-104, 28th *Inter. Conf. Elec. Prop.*, Toulouse, France, March 2003.
23. V. Kim, "About the influence of delay effects on the developments of low frequency oscillations in an accelerator with a closed drift and an extended acceleration zone", *4th All-Union Plasma Acceleration and Ion Injectors Conf*., pp. 61-62, Moscow, 1978 [in Russia].

24. V. Khayms and M. Martinez-Sanchez, "Design of a miniaturized Hall thruster", AIAA 96-3291, 32nd *Joint Prop. Conf., Lake Buena Vista*, FL., July 1996.

25. M.B. Belikov, O.A. Gorshkov,A.B. Jakupov, and S.A. Khartov., "Experimental Research of SPT Low-Power Perspective Model", AIAA-98-3786,*34th Joint propulsion Conf.,* Cleveland, OH, July 1998.

26. L. Zakharenkov, G. Chiskov, A. Semenkin, and T. Lawrence. IEPC-01-041, *Proc. Of the 27th International Electric Propulsion Conference,* Pasadena, California, October 2001.

27. Raitses, Y., Ashkenazy, J. and Appelbaum, G., "Probe Measurements of Plasma Properties Inside an Experimental Hall Thruster," AIAA-98-3640, *34th Joint propulsion Conf.,* Cleveland, OH, July 1998.

28. A. Warshavsky, I. Zur, J. Ashkenazy, G. Appelbaum, "Thermal Modeling and Measurements of an Engineering Model Hall Thruster", IEPC-03-21, 28th *Inter Conf. Elec. Prop.*, Toulouse, France, March 2003.

29. S. Gavril, "Ansys Analysis of the Magnetic Circuit", (in Hebrew), technical report TR-EHL-M-1500A/2, Manor Divisions Rafael, Israel, 2004.

30. A. Cohen-Zur, A. Fruchtman, J. Ashkenazy, A. Gany, "Analysis of the Steady State Axial Flow in the Hall Thruster", Vol. 9, *Physics of Plasmas,* October 2002.

31. N. Maslennikov, "Lifetime of the Stationary Plasma Thruster", IEPC-95-75, *Proc. of the 24th International Electric Propulsion Conference*, Moscow, Sept. 1995.

32. Y. Raitses, J. Ashkenazy and G. Appelbaum, "A High Resolution Thrust-Stand for Performance Tests of Hall Thrusters", Soreq NRC report 2301, Israel, August 1993.

33. J. Ashkenazy, A. Fruchtman, Y. Raitses and N. J. Fisch, "Modeling the behavior of Hall Current Plasma Accelerators", *Journal of Plasma Physics and Controlled Fusion*, 41, pp. 357-364, 1999.

34. J. Ashkenazy, G. Appelbaum, A. Kogan and M. Guelmann, "Torque Control of Hall Propelled Small Spacecraft", IEPC-99-183, *Proc. of the 26th Inter. Conf. Elec. Prop.*, Kitakyushu, Japan, October 1999.

35. L. Dorf, Y. Raitses, and N. J. Fisch, "Effect of anode dielectric coating on Hall thruster operation", *Applied Physics Letters* Vo.84 No.7, Feb. 2004.

36. J. R. Beatie, R. R. Robson and J. D. Williams, "18mN, xenon ion propulsion subsystem", IEPC-91-010, *22nd International Electric Propulsion Conf. Proc.*, Viarregio, Italy, Oct. 1991.

37. J. R. Stone, NASA, "Electrothermal Auxiliary Propulsion Technology", AIAA 86-1703, presented at the AIAA/SAE/ASME/ASEE 22nd *Joint Propulsion Conference*, Huntsville, AL, June 1986.

38. Dieter M. Zube, " First application of an arcjet thruster for the orbit control of a non-geostationary satellite", web page at the IRS, Germany, http://www.amsat.org/amsat/sats/phase3d/atos.html.

39. A. I. Morozov et al., "A study of ion formation in a Hall accelerator", Sov. Phys. Tech. Phys., 33(2), pp. 185-187, February 1988.

40. Richard Robert Hofer, "Development and Characterization of High Efficiency, High Specific Impulse Xenon Hall Thrusters", Research Thesis, 2004.

41. Kim, V., Popov, G., Kozlov, V., Skrylnikov, A., et al., "Investigation of SPT performance and particularities of its operation with Kr and Kr/Xe mixtures, "IEPC-01-065, *27th International Electric Propulsion Conference*, Pasadena, CA, Oct. 15-19, 2001.

42. Garrigues, L., Boniface., et al., "Parametric study of Hall thruster operation based on a 2D hybrid model: influence of the magnetic field on the thruster performance and lifetime," IEPC-2003-183, *28th International Electric Propulsion Conference*, Toulouse, France, March 17-21, 2003.